bioRxiv preprint doi: https://doi.org/10.1101/2020.07.30.229864; this version posted January 4, 2021. The copyright holder for this preprint (which was not certified by peer review) is the author/funder, who has granted bioRxiv a license to display the preprint in perpetuity. It is made available under aCC-BY-NC-ND 4.0 International license.

1 # CAR/Nr1i3 directs T cell adaptation to bile acids in the small
2 # intestine

3 **Mei Lan Chen[1,2#], Xiangsheng Huang[3#], Hongtao Wang[3], Courtney Hegner[1,2], Yujin Liu[1], Jinsai**
4 **Shang[4], Amber Eliason[1], HaJeung Park[5], Blake Frey[6], Guohui Wang[3], Sarah A. Mosure[1,2,4],**
5 **Laura A. Solt[1,4], Douglas J. Kojetin[4,7], Alex Rodriguez-Palacios[8,9], Deborah A. Schady[10], Casey T.**
6 **Weaver[6], Matthew E. Pipkin[1], David D. Moore[11^]*, and Mark S. Sundrud[1]***

7 [1]Department of Immunology and Microbiology, The Scripps Research Institute, Jupiter, FL 33458,
8 USA

9 [2]Skaggs Graduate School of Chemical and Biological Sciences, The Scripps Research Institute,
10 Jupiter, FL, 33458, USA.

11 [3]Section of Gastroenterology, Hepatology, and Nutrition, Department of Pediatrics, Baylor College of
12 Medicine and Texas Children's Hospital, Houston, TX, 77030, USA

13 [4]Department of Integrative Structural and Computational Biology, The Scripps Research Institute,
14 Jupiter, FL 33458, USA

15 [5]X-ray Crystallography Core Facility, The Scripps Research Institute, Jupiter, FL 33458, USA

16 [6]Department of Pathology, University of Alabama at Birmingham, Birmingham, AL 35203, USA

17 [7]Department of Molecular Medicine, The Scripps Research Institute, Jupiter, FL 33458, USA

18 [8]Division of Gastroenterology and Liver Disease, School of Medicine, Case Western Reserve
19 University, Cleveland, OH 44106, USA

20 [9]University Hospitals Research and Education Institute, University Hospitals Cleveland Medical
21 Center, Cleveland, OH 44106, USA

22 [10]Department of Pathology and Immunology, Texas Children's Hospital, Baylor College of Medicine,
23 Houston, TX 77030, USA.

24 [11]Department of Molecular and Cellular Biology, Baylor College of Medicine, 1 Baylor Plaza,
25 Houston, TX 77030, USA

26 [#]Equal contribution

27 [^]Current address: Department of Nutritional Sciences and Toxicology, University of California
28 Berkeley, Berkeley, CA 94720, USA
29

30 **Key words**: IBD, T cells, Th1, Th17, bile acids, MDR1, CAR, NR1I3, xenobiotics

31 **Abbreviations**: MDR1, multidrug resistance 1; IFNγ, interferon gamma; IL-10, interleukin-10; IL-17,
32 interleukin-17; *Abcb1a*, ATP-binding cassette subfamily B, member 1a; *Abcb1b*, ATP-binding cassette
33 subfamily B, member 1b; *Rag1/2*, recombination-activating gene 1 or 2.

bioRxiv preprint doi: https://doi.org/10.1101/2020.07.30.229864; this version posted January 4, 2021. The copyright holder for this preprint (which was not certified by peer review) is the author/funder, who has granted bioRxiv a license to display the preprint in perpetuity. It is made available under aCC-BY-NC-ND 4.0 International license.

34 **Bile acids (BAs) are lipid emulsifying metabolites synthesized in hepatocytes and maintained *in*
35 *vivo* through enterohepatic circulation between the liver and small intestine[1]. As detergents, BAs
36 can cause toxicity and inflammation in enterohepatic tissues[2]. Nuclear receptors maintain BA
37 homeostasis in hepatocytes and enterocytes[3], but it is unclear how mucosal immune cells tolerate
38 high BA concentrations in the small intestine lamina propria (siLP). We previously reported that
39 CD4$^+$ T effector (Teff) cells upregulate expression of the xenobiotic transporter MDR1/*ABCB1* in
40 the siLP to prevent BA toxicity and suppress Crohn's disease-like small bowel inflammation[4].
41 Here, we identify the nuclear xenobiotic receptor, constitutive androstane receptor
42 (CAR/*NR1I3*), as a regulator of MDR1 expression in T cells, and safeguard against BA toxicity
43 and inflammation in the small intestine. CAR was activated and induced large-scale
44 transcriptional reprograming in Teff cells infiltrating the siLP, but not the colon. CAR induced
45 expression of detoxifying enzymes and transporters in siLP Teff cells, as in hepatocytes, but also
46 the key anti-inflammatory cytokine, *Il10*. Accordingly, CAR-deficiency in T cells exacerbated,
47 whereas pharmacologic CAR activation suppressed, BA-driven ileitis in T cell-
48 reconstituted *Rag*$^{-/-}$ mice. These data suggest that CAR acts locally in small intestinal T cells to
49 detoxify BAs and resolve inflammation. Activation of this program offers an unexpected strategy
50 to treat small bowel Crohn's disease, and provides evidence of lymphocyte sub-specialization
51 within the small intestine.**

52 Seeking transcriptional mechanisms underlying MDR1 upregulation in siLP Teff cells[4], we
53 considered the ligand-regulated nuclear receptors (NRs), a family of environmental-sensing
54 transcription factors that control diverse gene expression programs important for immunity,
55 inflammation, metabolism and gastrointestinal physiology[5]. To assess functions of all 49 mouse NRs,
56 their individual contributions to mucosal Teff cell MDR1 expression were assessed in a pooled *in vivo*
57 RNAi screen. Activated naïve CD4$^+$ T cells transduced separately with 258 retroviruses expressing
58 shRNAmirs against 70 genes (Supplemental Table 1) were pooled, FACS-sorted for retroviral reporter
59 (Ametrine) expression, and transferred into syngeneic (FVB/N, 'FVB') *Rag1*$^{-/-}$ mice. Six-weeks later,
60 transduced Teff cells were recovered from spleen or siLP, and MDR1^{hi} or MDR1^{lo} subsets were
61 isolated based on *ex vivo* efflux of the fluorescent MDR1 transport substrate, rhodamine 123 (Rh123)[6].
62 shRNAmir abundances were quantified by DNA-seq (**Fig. 1a**).

63 Multiple shRNAmirs against constitutive androstane receptor (CAR/*Nr1i3*) and MDR1/*Abcb1a*
64 itself were enriched in MDR1^{lo} *vs*. MDR1^{hi} Teff cells from both spleen and siLP (**Fig. 1b**; Extended
65 Data Fig. 1a-b). As CAR prevents BA-induced hepatotoxicity[8], and regulates hepatic MDR1
66 expression[9], these results suggested CAR might have similar protective functions in Teff cells

bioRxiv preprint doi: https://doi.org/10.1101/2020.07.30.229864; this version posted January 4, 2021. The copyright holder for this preprint (which was not certified by peer review) is the author/funder, who has granted bioRxiv a license to display the preprint in perpetuity. It is made available under aCC-BY-NC-ND 4.0 International license.

67 infiltrating the siLP. We confirmed 3 of 5 CAR/*Nr1i3*-specific shRNAmirs reduced MDR1-dependent
68 Rh123 efflux in Teff cells recovered from transferred *Rag1*$^{-/-}$ mice (**Fig. 1c**, Extended Data Fig. 1c-d).
69 These same clones silenced CAR/*Nr1i3* expression, as judged by *ex vivo* qPCR, and reduced
70 expression of both MDR1/*Abcb1a* and the signature CAR target gene, *Cyp2b10*[10] (Extended Data Fig.
71 1e).

72 CAR regulates transcription as a heterodimer with retinoid X receptors (RXRα/β/γ)[11].
73 However, RXRs also dimerize with other NRs that regulate diverse aspects of T cell function *in vivo*[11].
74 Accordingly, shRNAmir-mediated RXRα depletion predominantly impacted Teff cell persistence *in*
75 *vivo* (Extended Data Fig. 1f). Depletion of the CAR-related xenobiotic-sensor, pregnane X receptor
76 (PXR/*Nr1i2*)[12], had little influence on either MDR1 expression or Teff cell persistence (**Fig. 1b**;
77 Extended Data Fig. 1f). Consistent with this, Teff cells from C57BL/6 (B6)-derived CAR-deficient
78 (*Nr1i3*$^{-/-}$) mice, but not PXR-deficient (*Nr1i2*$^{-/-}$) mice, displayed lower MDR1 expression than
79 bystander CD45.1 wild type cells after co-transfer into *Rag1*$^{-/-}$ mice; cells lacking only CAR showed
80 equivalently low MDR1 expression as those lacking both CAR and PXR (Extended Data Fig. 1g-i).
81 These data implicate CAR in the regulation of mucosal T cell function *in vivo*.

82 The degree to which shRNAmir-mediated CAR depletion attenuated MDR1 expression in FVB
83 wild type Teff cells transplanted into *Rag1*$^{-/-}$ mice correlated directly with the severity of weight loss
84 these cells induced (**Fig. 1d-e**; Extended data Fig. 1c-d). This was consistent with our prior observation
85 that FVB T cells lacking MDR1 (*Abcb1a*$^{-/-}$*Abcb1b*$^{-/-}$) induce more severe weight loss than wild type
86 counterparts in reconstituted *Rag1*$^{-/-}$ mice—due to induction of both colitis and BA-driven ileitis[4]—
87 and is distinct from wild type naïve CD4^{+} T cells, which induce only colitis in immunodeficient
88 hosts[13]. Naive T cells from B6-derived CAR-deficient mice also produced increased weight loss and
89 ileitis than wild type counterparts, but equivalent colitis, after transfer into *Rag2*$^{-/-}$ mice co-housed to
90 normalize microflora (**Fig. 1f-h**). Therapeutic administration of cholestyramine (CME)[14], a BA
91 sequestering resin that prevents BA reabsorption into the siLP, normalized weight loss and ileitis
92 between *Rag2*$^{-/-}$ recipients of wild type or CAR-deficient T cells (Extended Data Fig. 2a-b); as did
93 ablation of the ileal BA reuptake transporter, Apical sodium-dependent BA transporter
94 (Asbt/*Slc10a2*)[15], in *Rag1*$^{-/-}$ recipients (Extended Data Fig. 2c-d). Neither genetic nor pharmacologic
95 inhibition of ileal BA reabsorption affected severity of T cell transfer-induced colitis (Extended Data
96 Fig. 2b, 2d). These results suggest CAR acts selectively in T cells to regulate small bowel immune
97 homeostasis; CAR-deficiency in T cells exacerbates ileitis that is not transmissible by microbiota and
98 requires BA reabsorption.

bioRxiv preprint doi: https://doi.org/10.1101/2020.07.30.229864; this version posted January 4, 2021. The copyright holder for this preprint (which was not certified by peer review) is the author/funder, who has granted bioRxiv a license to display the preprint in perpetuity. It is made available under aCC-BY-NC-ND 4.0 International license.

99 To elucidate CAR-dependent transcriptional programs in T cells, bystander CD45.1 wild type
100 and CD45.2 CAR-deficient Teff cells were purified from spleen, siLP or colon lamina propria (cLP) of
101 co-transferred *Rag1*$^{-/-}$ mice and analyzed by RNA-seq (**Fig. 2a**). Gene expression in wild type Teff
102 cells differed substantially between spleen, siLP and cLP, whereas CAR-deficiency most
103 conspicuously altered gene expression in siLP Teff cells (**Fig. 2b**). CAR-deficient siLP Teff cells
104 failed to upregulate many 'siLP-signature' genes preferentially expressed in wild type cells from siLP
105 *vs*. either spleen or cLP, and ectopically expressed genes characteristic of wild type Teff cells from
106 colon (**Fig. 2c-d**). siLP-signature genes encoding chaperones, receptors and enzymes involved in lipid
107 binding, transport and metabolism (*e.g*., *Apold1*, *Pex26*, *Dgkh*, *Ldlr*, *Phyhd1*, *Lclat1*) were among
108 those decreased in CAR-deficient *vs*. wild type siLP Teff cells (**Fig. 2c-d**, Supplemental Table 2); as
109 were genes induced by CAR in mouse hepatocytes after *in vivo* administration of the specific agonist
110 ligand, 1,4-*Bis*(3,5-Dichloro-2-pyridinyloxy) benzene (TCPOBOP, 'TC')[16] (Extended Data Fig. 3a-b).
111 Genes showing CAR-dependent expression in both siLP Teff cells and hepatocytes were enriched for
112 loci at which TC-inducible CAR DNA-binding has been observed in hepatocytes by ChIP-seq[17]
113 (Extended Data Fig. 3c). These included MDR1/*Abcb1a* and *Cyp2b10*, as expected, but also other
114 ABC-family transporters (*e.g*., *Abcb4*) and cytochrome P450 enzymes (*e.g*., *Cyp2r1*) (Extended Data
115 Fig. 3d), suggesting that CAR activates a 'hepatocyte-like' BA-detoxification program in siLP Teff
116 cells. CAR-deficient Teff cells accumulated less in the siLP of *Rag1*$^{-/-}$ recipients initially, and in all
117 tissues later, relative to wild type bystanders (Extended Data Fig. 4a-c). Ablating Asbt-dependent BA
118 reabsorption in *Rag1*$^{-/-}$ recipients tended to minimize this phenotype (Extended Data Fig. 4d-f).

119 To test if CAR also regulates small intestine-associated T cell function in humans, we analyzed
120 CAR expression and function in healthy adult peripheral blood T cell subsets most likely to have
121 recirculated from the siLP. 1-5% of circulating Teff cells expressed the requisite combination of
122 receptors for siLP-homing, α4β7 integrin and CCR9[18] ($\alpha4^+\beta7^+$CCR9$^+$), whereas naïve T cells that lack
123 gut-homing potential did not (Extended Data Fig. 5a-c). Fewer CD25$^+$ T regulatory (Treg) cells
124 expressed these receptors (Extended Data Fig. 5a-c), suggesting Treg cells may be more efficiently
125 retained in the siLP than Teff cells. As predicted, siLP-linked $\alpha4^+\beta7^+$CCR9$^+$ Teff cells displayed
126 elevated expression of MDR1/*ABCB1*, CAR/*NR1I3* and *CYP2B6* (ortholog of mouse *Cyp2b10*[19]),
127 compared with naïve, Treg or Teff cells lacking one or more siLP-homing receptors (Extended Data
128 Fig. 5d-f). In addition, only $\alpha4^+\beta7^+$CCR9$^+$ Teff cells responded to *ex vivo* treatment with the human
129 CAR agonist ligand, 6-(4-Chlorophenyl)imidazo[2,1-b][1,3]thiazole-5-carbaldehyde O-(3,4-
130 dichlorobenzyl) oxime (CITCO)[19] by upregulating *CYP2B6* and *ABCB1* (Extended Data Fig. 5g-h).

bioRxiv preprint doi: https://doi.org/10.1101/2020.07.30.229864; this version posted January 4, 2021. The copyright holder for this preprint (which was not certified by peer review) is the author/funder, who has granted bioRxiv a license to display the preprint in perpetuity. It is made available under aCC-BY-NC-ND 4.0 International license.

131 $CCR6^{+}CXCR3^{hi}CCR4^{lo}$ "Th17.1" cells—which possess both Th17 and Th1 effector functions, and
132 high MDR1 expression[20]—were enriched among total $\alpha4^{+}\beta7^{+}CCR9^{+}$ Teff cells (Extended Data Fig.
133 5i-l). However, $\alpha4^{+}\beta7^{+}CCR9^{+}$ Th17.1 cells exhibited higher MDR1 expression than Th17.1 cells
134 lacking one or more siLP-homing receptors (Extended Data Fig. 5m-n). The same was true for Th17
135 ($CCR6^{+}CXCR3^{lo}CCR4^{hi}$) and Th1 ($CCR6^{-}CXCR3^{hi}$ $CCR4^{lo}$) cells. These data suggest that CAR
136 preferentially operates in both mouse and human Teff cells in the small intestine.

137 Preferential CAR function in siLP Teff cells could involve local activation by endogenous
138 metabolites. Consistent with this possibility, gallbladder bile or sterile-filtered soluble small intestine
139 lumen content (siLC) from wild type B6 mice—but not colon lumen content (cLC) or serum—induced
140 MDR1/*Abcb1a* and *Cyp2b10* upregulation in *ex vivo*-stimulated wild type, but not CAR-deficient, Teff
141 cells from transferred *Rag1*$^{-/-}$ mice (**Fig. 2e**; Extended Data Fig. 6a). CAR-dependent gene expression
142 in this *ex vivo* culture system was also induced by TC, inhibited by the CAR inverse agonist, 5α-
143 Androstan-3β-ol[8], and unaffected by the PXR agonist, 5-Pregnen-3β-ol-20-one-16α-carbonitrile
144 (PCN)[12] (**Fig. 2e**; Extended Data Fig. 6b). Bile and siLC concentrations that enhanced CAR-dependent
145 gene expression in Teff cells also promoted recruitment of a PGC1α co-activator peptide to
146 recombinant CAR-RXRα ligand-binding domain (LBD) heterodimers, but not to RXRα LBD
147 homodimers, in time-resolved fluorescence resonance energy transfer (TR-FRET) experiments (**Fig.
148 2f-g**; Extended Data Fig. 7a-b). As CAR is thought to indirectly sense, but not directly bind major BA
149 species[21], we reasoned that biliary metabolites other than BAs might activate the CAR LBD; bile is
150 comprised of mixed micelles containing BAs, phospholipids, cholesterol, fatty acids and bile pigments
151 (*e.g.*, bilirubin)[1]. Indeed, siLC pre-treated with CME to deplete free BAs[4] retained capacity to activate
152 CAR-RXRα LBD heterodimers (Extended Data Fig. 7c). Further, no major BA species activated
153 CAR-RXRα LBD heterodimers in TR-FRET experiments, or stimulated CAR-dependent gene
154 expression in *ex vivo*-cultured Teff cells (Extended Data Fig. 7d, data not shown). siLC from germ-free
155 mice also activated CAR-RXRα LBD heterodimers (Extended Data Fig. 7c, data not shown), together
156 suggesting that host-derived, non-BA constituents of bile may stimulate local CAR transcriptional
157 activity in siLP Teff cells.

158 To further explore CAR immunoregulatory functions, we examined its control of gene
159 expression associated with major pro- and anti-inflammatory T helper cell lineages. Genes expressed
160 selectively in type 1 regulatory (Tr1) cells[22]—a $Foxp3^{-}IL\text{-}10^{+}$ subset known for suppressing mucosal
161 inflammation in humans and mice[23]—were enriched among those showing reduced expression in
162 CAR-deficient *vs.* wild type siLP Teff cells (**Fig. 3a-c**). Conversely, genes characteristic of pro-

bioRxiv preprint doi: https://doi.org/10.1101/2020.07.30.229864; this version posted January 4, 2021. The copyright holder for this preprint (which was not certified by peer review) is the author/funder, who has granted bioRxiv a license to display the preprint in perpetuity. It is made available under aCC-BY-NC-ND 4.0 International license.

163 inflammatory IL-17-secreting (Th17) cells[24] were positively enriched within siLP Teff cells lacking
164 CAR (**Fig. 3b**). In line with these signatures, CAR-deficient Teff cells inefficiently expressed both a
165 *Thy1.1*-expressing *Il10* reporter ('10BiT'[25]; **Fig. 3d-e**), and endogenous IL-10 protein (Extended Data
166 Fig. 8a-e), after transfer into *Rag1*$^{-/-}$ mice. Reduced *Il10* expression in Teff cells lacking CAR
167 paralleled their accumulation as RORγt^{+}IL-17A^{-} 'poised' Th17 cells[26,27] in siLP (Extended Data Fig.
168 8f-g). However, *Il10*$^{-/-}$ T cells replete for CAR recapitulated this phenotype (Extended Data Fig. 8h-i),
169 suggesting that CAR may reciprocally regulate Tr1 and Th17 cell development in the siLP via IL-10
170 induction. TC (synthetic CAR agonist), as well as bile and siLC from wild type mice, each promoted
171 *Il10* upregulation in *ex vivo*-stimulated wild type, but not CAR-deficient, Teff cells (**Fig. 3f**; Extended
172 Data Fig. 6), akin to *Abcb1a* and *Cyp2b10* (**Fig. 2e**).

173 CAR-dependent IL-10 expression in T cell-reconstituted *Rag1*$^{-/-}$ mice was transient—peaking
174 2-weeks after donor T cell engraftment and waning thereafter—and followed the kinetics of both Teff
175 cell siLP infiltration and *ex vivo* CAR (*Nr1i3*), MDR1 (*Abcb1a*) and *Cyp2b10* gene expression
176 (Extended Data Fig. 9a-c). This suggested that CAR expression and function in Teff cells is increased
177 in response to inflammation, analogous to Tr1 cell dynamics *in vivo*[28]. Using an orthologous approach
178 to induce intestinal inflammation in wild type or CAR-deficient mice—soluble anti-CD3 injection[23]—
179 we confirmed that CAR was required for anti-CD3 (*i.e*., inflammation)-induced IL-10 upregulation by
180 endogenous effector and regulatory T cell subsets in the siLP, but not the spleen, and was dispensable
181 for steady-state IL-10 expression in T cells from unmanipulated mice (Extended data Figure 9d-f).

182 To establish a model of CAR-dependent Tr1 cell function *in vitro*, we tested CAR expression
183 and function in naïve CD4^{+} T cells activated and expanded in culture conditions previously reported to
184 induce differentiation of Foxp3^{-}IL-10^{+} 'Tr1-like' cells. Combining IL-27—a cytokine that promotes
185 Stat3-dependent IL-10 expression[22]—with the synthetic corticosteroid, dexamethasone (Dex)[29],
186 strongly induced CAR/*Nr1i3* and IL-10 expression, but not Foxp3 expression, in activated T cells (**Fig.
187 3g-I**, data not shown). Loss of CAR impaired IL-10 production by IL-27+Dex-elicited Tr1-like cells
188 (**Fig. 3h-i**). By contrast, CAR/*Nr1i3* expression remained low during *in vitro* development of other
189 effector (*e.g*., Th1, Th2, Th17) or Foxp3^{+} induced (i)Treg lineages, and CAR ablation had little impact
190 on the development or function of these cells (**Fig. 3g**, Supplemental Table 3). Together, these results
191 suggest CAR is essential for *Il10* gene regulation in Tr1 cells, which may synergize with CAR-
192 dependent BA-detoxification to enforce small bowel immune homeostasis.

193 Finally, we reasoned that if CAR-deficiency in Teff cells exacerbates BA-driven small bowel
194 inflammation, pharmacologic CAR activation might be protective. A single administration of the CAR

bioRxiv preprint doi: https://doi.org/10.1101/2020.07.30.229864; this version posted January 4, 2021. The copyright holder for this preprint (which was not certified by peer review) is the author/funder, who has granted bioRxiv a license to display the preprint in perpetuity. It is made available under aCC-BY-NC-ND 4.0 International license.

195 agonist, TC, to *Rag1*$^{-/-}$ mice reconstituted with a mixture of CD45.1 wild type and CD45.2 CAR-
196 deficient T cells induced *Abcb1a*, *Cyp2b10* and *Il10* upregulation in wild type, but not CAR-deficient,
197 Teff cells within 72 hr (**Fig. 4a**). Weekly TC administration reduced ileitis, but not colitis, in *Rag2*$^{-/-}$
198 mice reconstituted with only wild type T cells and fed a standard 0.2% cholic acid (CA)-supplemented
199 diet to increase the circulating BA pool and promote small bowel injury[8,12] (**Fig. 4b-c**). CA-feeding
200 increased morbidity in *Rag2*$^{-/-}$ mice receiving wild type T cells, but had no obvious effects on *Rag2*$^{-/-}$
201 mice in the absence of T cell transfer (**Fig. 4b**). Therapeutic effects of TC were abolished in CA-fed
202 *Rag2*$^{-/-}$ mice reconstituted with CAR-deficient T cells (Extended Data Fig. 10), together suggesting
203 that BA-supplementation promotes, whereas CAR activation in T cells suppresses, experimental ileitis.
204 Enterohepatic circulation establishes a marked concentration gradient of BAs in the small
205 intestine (millimolar) and colon (micromolar), which opposes that of bacteria and bacterial
206 metabolites[1]. While antigens from enteric flora prime both pro- and anti-inflammatory T cell responses
207 across the intestinal tract, the specific requirement for CAR-function in siLP Teff cells—defined here
208 in an *in vivo* screen, and relative to other NRs with known regulatory functions in the colon (*e.g.*,
209 vitamin D receptor, 'VDR')[30]—suggests important distinctions between the immunoregulatory
210 microenvironments of the small and large intestines. Opposing concentration gradients of bile and
211 bacteria in the small and large intestines could be sensed by distinct sets of NRs in mucosal
212 lymphocytes, and instruct compartmentalized regulatory functions. Microbe-induced Foxp3^{+} Treg cell
213 development and function, for example, is most prominent in the colon and involves VDR[30]. By
214 contrast, we show here that the BA- and xenobiotic-sensing nuclear receptor, CAR/Nr1i3, redirects
215 gene expression in Foxp3^{-} Teff cells infiltrating the small intestine, but not the colon, to counter BA-
216 induced toxicity and inflammation (**Fig. 4d**). Pharmacologic CAR activation could offer a new, more
217 targeted, approach for treating small bowel Crohn's disease, while also providing insight into
218 lymphocyte specialization across the intestinal tract.
219

bioRxiv preprint doi: https://doi.org/10.1101/2020.07.30.229864; this version posted January 4, 2021. The copyright holder for this preprint (which was not certified by peer review) is the author/funder, who has granted bioRxiv a license to display the preprint in perpetuity. It is made available under aCC-BY-NC-ND 4.0 International license.

220 **References**

221 1 Hofmann, A. F. & Hagey, L. R. Key discoveries in bile acid chemistry and biology and their
222 clinical applications: history of the last eight decades. *Journal of lipid research* **55**, 1553-1595,
223 doi:10.1194/jlr.R049437 (2014).
224 2 Poupon, R., Chazouilleres, O. & Poupon, R. E. Chronic cholestatic diseases. *J Hepatol* **32**, 129-
225 140 (2000).
226 3 Arab, J. P., Karpen, S. J., Dawson, P. A., Arrese, M. & Trauner, M. Bile acids and nonalcoholic
227 fatty liver disease: Molecular insights and therapeutic perspectives. *Hepatology* **65**, 350-362,
228 doi:10.1002/hep.28709 (2017).
229 4 Cao, W. *et al.* The Xenobiotic Transporter Mdr1 Enforces T Cell Homeostasis in the Presence
230 of Intestinal Bile Acids. *Immunity* **47**, 1182-1196 e1110, doi:10.1016/j.immuni.2017.11.012
231 (2017).
232 5 Lazar, M. A. Maturing of the nuclear receptor family. *J Clin Invest* **127**, 1123-1125,
233 doi:10.1172/JCI92949 (2017).
234 6 Ludescher, C. *et al.* Detection of activity of P-glycoprotein in human tumour samples using
235 rhodamine 123. *British journal of haematology* **82**, 161-168 (1992).
236 7 Pols, T. W., Noriega, L. G., Nomura, M., Auwerx, J. & Schoonjans, K. The bile acid
237 membrane receptor TGR5 as an emerging target in metabolism and inflammation. *J Hepatol*
238 **54**, 1263-1272, doi:10.1016/j.jhep.2010.12.004 (2011).
239 8 Zhang, J., Huang, W., Qatanani, M., Evans, R. M. & Moore, D. D. The constitutive androstane
240 receptor and pregnane X receptor function coordinately to prevent bile acid-induced
241 hepatotoxicity. *J Biol Chem* **279**, 49517-49522, doi:10.1074/jbc.M409041200 (2004).
242 9 Cerveny, L. *et al.* Valproic acid induces CYP3A4 and MDR1 gene expression by activation of
243 constitutive androstane receptor and pregnane X receptor pathways. *Drug Metab Dispos* **35**,
244 1032-1041, doi:10.1124/dmd.106.014456 (2007).
245 10 Wei, P., Zhang, J., Egan-Hafley, M., Liang, S. & Moore, D. D. The nuclear receptor CAR
246 mediates specific xenobiotic induction of drug metabolism. *Nature* **407**, 920-923,
247 doi:10.1038/35038112 (2000).
248 11 Evans, R. M. & Mangelsdorf, D. J. Nuclear Receptors, RXR, and the Big Bang. *Cell* **157**, 255-
249 266, doi:10.1016/j.cell.2014.03.012 (2014).

bioRxiv preprint doi: https://doi.org/10.1101/2020.07.30.229864; this version posted January 4, 2021. The copyright holder for this preprint (which was not certified by peer review) is the author/funder, who has granted bioRxiv a license to display the preprint in perpetuity. It is made available under aCC-BY-NC-ND 4.0 International license.

250 12 Staudinger, J. L. *et al.* The nuclear receptor PXR is a lithocholic acid sensor that protects
251 against liver toxicity. *Proc Natl Acad Sci U S A* **98**, 3369-3374, doi:10.1073/pnas.051551698
252 (2001).
253 13 Ostanin, D. V. *et al.* T cell transfer model of chronic colitis: concepts, considerations, and
254 tricks of the trade. *American journal of physiology. Gastrointestinal and liver physiology* **296**,
255 G135-146, doi:10.1152/ajpgi.90462.2008 (2009).
256 14 Arnold, M. A. *et al.* Colesevelam and Colestipol: Novel Medication Resins in the
257 Gastrointestinal Tract. *The American journal of surgical pathology*,
258 doi:10.1097/PAS.0000000000000260 (2014).
259 15 Dawson, P. A., Lan, T. & Rao, A. Bile acid transporters. *Journal of lipid research* **50**, 2340-
260 2357, doi:10.1194/jlr.R900012-JLR200 (2009).
261 16 Cui, J. Y. & Klaassen, C. D. RNA-Seq reveals common and unique PXR- and CAR-target gene
262 signatures in the mouse liver transcriptome. *Biochim Biophys Acta* **1859**, 1198-1217,
263 doi:10.1016/j.bbagrm.2016.04.010 (2016).
264 17 Niu, B. *et al.* In vivo genome-wide binding interactions of mouse and human constitutive
265 androstane receptors reveal novel gene targets. *Nucleic Acids Res* **46**, 8385-8403,
266 doi:10.1093/nar/gky692 (2018).
267 18 De Calisto, J. *et al.* T-cell homing to the gut mucosa: general concepts and methodological
268 considerations. *Methods Mol Biol* **757**, 411-434, doi:10.1007/978-1-61779-166-6_24 (2012).
269 19 Maglich, J. M. *et al.* Identification of a novel human constitutive androstane receptor (CAR)
270 agonist and its use in the identification of CAR target genes. *J Biol Chem* **278**, 17277-17283,
271 doi:10.1074/jbc.M300138200 (2003).
272 20 Ramesh, R. *et al.* Pro-inflammatory human Th17 cells selectively express P-glycoprotein and
273 are refractory to glucocorticoids. *J Exp Med* **211**, 89-104, doi:10.1084/jem.20130301 (2014).
274 21 Moore, L. B. *et al.* Pregnane X receptor (PXR), constitutive androstane receptor (CAR), and
275 benzoate X receptor (BXR) define three pharmacologically distinct classes of nuclear receptors.
276 *Mol Endocrinol* **16**, 977-986, doi:10.1210/mend.16.5.0828 (2002).
277 22 Karwacz, K. *et al.* Critical role of IRF1 and BATF in forming chromatin landscape during type
278 1 regulatory cell differentiation. *Nat Immunol* **18**, 412-421, doi:10.1038/ni.3683 (2017).
279 23 Gagliani, N. *et al.* Coexpression of CD49b and LAG-3 identifies human and mouse T
280 regulatory type 1 cells. *Nat Med* **19**, 739-746, doi:10.1038/nm.3179 (2013).
281 24 Korn, T., Bettelli, E., Oukka, M. & Kuchroo, V. K. IL-17 and Th17 Cells. *Annu Rev Immunol*
282 **27**, 485-517, doi:10.1146/annurev.immunol.021908.132710 (2009).

bioRxiv preprint doi: https://doi.org/10.1101/2020.07.30.229864; this version posted January 4, 2021. The copyright holder for this preprint (which was not certified by peer review) is the author/funder, who has granted bioRxiv a license to display the preprint in perpetuity. It is made available under aCC-BY-NC-ND 4.0 International license.

283 25 Maynard, C. L. *et al.* Regulatory T cells expressing interleukin 10 develop from Foxp3+ and
284 Foxp3- precursor cells in the absence of interleukin 10. *Nat Immunol* **8**, 931-941,
285 doi:10.1038/ni1504 (2007).
286 26 Sano, T. *et al.* An IL-23R/IL-22 Circuit Regulates Epithelial Serum Amyloid A to Promote
287 Local Effector Th17 Responses. *Cell* **163**, 381-393, doi:10.1016/j.cell.2015.08.061 (2015).
288 27 Wan, Q. *et al.* Cytokine signals through PI-3 kinase pathway modulate Th17 cytokine
289 production by CCR6+ human memory T cells. *J Exp Med* **208**, 1875-1887,
290 doi:10.1084/jem.20102516 (2011).
291 28 Yadava, K. *et al.* Natural Tr1-like cells do not confer long-term tolerogenic memory. *Elife* **8**,
292 doi:10.7554/eLife.44821 (2019).
293 29 Barrat, F. J. *et al.* In vitro generation of interleukin 10-producing regulatory CD4(+) T cells is
294 induced by immunosuppressive drugs and inhibited by T helper type 1 (Th1)- and Th2-
295 inducing cytokines. *J Exp Med* **195**, 603-616, doi:10.1084/jem.20011629 (2002).
296 30 Song, X. *et al.* Microbial bile acid metabolites modulate gut RORgamma(+) regulatory T cell
297 homeostasis. *Nature* **577**, 410-415, doi:10.1038/s41586-019-1865-0 (2020).

bioRxiv preprint doi: https://doi.org/10.1101/2020.07.30.229864; this version posted January 4, 2021. The copyright holder for this preprint (which was not certified by peer review) is the author/funder, who has granted bioRxiv a license to display the preprint in perpetuity. It is made available under aCC-BY-NC-ND 4.0 International license.

298 **Figure legends**

299 **Fig. 1. CAR/Nr1i3 regulates MDR1 expression in mucosal CD4$^+$ T cells. (a)** Schematic outline of
300 the pooled *in vivo* RNAi screening approach (see Methods for details). **(b)** Median $\log_2$ fold-change in
301 shRNAmir abundances in MDR1^{hi} *vs*. MDR1^{lo} siLP Teff cells, determined by DNA-seq and grouped
302 by gene (see Supplemental Table 1 for the list of shRNAmirs used in the screen). Horizontal lines
303 indicate 2-fold changes. **(c)** Diagram of the *Nr1i3*/CAR locus. Position of seed sequences for each
304 CAR/*Nr1i3*-specific shRNAmir is shown; 5' and 3' untranslated regions (UTR); filled boxes depict
305 exons. **(d)** Mean weight loss (+ SEM) in co-housed FVB.*Rag1*$^{-/-}$ mice receiving FVB wild type CD4$^+$
306 T cells expressing negative control *shCd8a* (n = 11), or CAR/*Nr1i3*-specific shRNAmirs; *shNr1i3.1* (n
307 = 7), *shNr1i3.2* (n = 7), *shNr1i3.3* (n = 7), *shNr1i3.4* (n = 7), *shNr1i3.5* (n = 7). ***P < .001, ****P <
308 .0001, Two-way ANOVA. Data from two experiments. **(e)** Correlation between severity of T cell
309 transfer-induced weight loss (at 6-weeks post-T cell transfer; as in [d]) and MDR1-dependent Rh123
310 efflux in *ex vivo*-isolated spleen Teff cells (determined by flow cytometry; see Extended Data Fig. 1c-
311 d). **P < .01, Pearson correlation test. **(f)** Mean weight loss (+ SEM) in co-housed B6.*Rag2*$^{-/-}$
312 recipients of C57BL/6 wild type (B6; blue; n = 7) or CAR-deficient (B6.*Nr1i3*$^{-/-}$; red; n = 9) naïve
313 CD4$^+$ T cells. **P < .01, Two-way ANOVA. Data from two experiments. **(g)** H&E-stained sections of
314 colons or terminal ilea from transferred B6.*Rag2*$^{-/-}$ mice (at 6-weeks post-T cell transfer; as in [f]).
315 Representative of 7-9 mice per group analyzed over two experiments. **(h)** Mean histology scores (+
316 SEM) for colons or terminal ilea as in (f-g). B6.*Rag2*$^{-/-}$ mice receiving wild-type (B6; n =7) or CAR-
317 deficient (B6.*Nr1i3*$^{-/-}$; n = 9) T cells *P < .01, unpaired two-tailed student's t test.

318

319 **Fig. 2. CAR regulates T cell gene expression in the small intestine. (a)** Mixed T cell transfer
320 approach for RNA-seq analysis of wild type (B6) and CAR-deficient (B6.*Nr1i3*$^{-/-}$) T effector (Teff)
321 cells. **(b)** PCA of wild type and CAR-deficient Teff cell gene expression in spleen, small intestine
322 lamina propria (siLP) or colon lamina propria (cLP). **(c)** *Top*, identification of signature (sig) genes
323 expressed highest in spleen, siLP or cLP wild type Teff cells. Comparisons, and numbers of genes
324 higher (sample 1/2) in each comparison, are listed. *Bottom*, differential gene expression between
325 spleen, siLP or cLP wild type and CAR-deficient Teff cells. Numbers of Up/Down genes are indicated.
326 Tissue-specific Teff cell-signature genes are highlighted/annotated. **(d)** *Left*, enrichment of tissue-
327 specific Teff cell-signature genes (x-axis; as in [c]) within those differentially expressed between wild
328 type and CAR-deficient cells per tissue (y-axis). *Right*, Gene ontology (GO) terms enriched in CAR-
329 dependent siLP Teff signature genes; lipid metabolic pathways highlighted red. (b-d) Gene expression

bioRxiv preprint doi: https://doi.org/10.1101/2020.07.30.229864; this version posted January 4, 2021. The copyright holder for this preprint (which was not certified by peer review) is the author/funder, who has granted bioRxiv a license to display the preprint in perpetuity. It is made available under aCC-BY-NC-ND 4.0 International license.

330 data from 3-independent experiments. **(e)** Mean relative *Abcb1a* or *Cyp2b10* expression ($\pm$ SEM; n =
331 3), by qPCR, in *ex vivo*-isolated wild type or CAR-deficient Teff cells stimulated +/- mouse tissue
332 extracts. Veh, vehicle; TC, TCPOBOP (CAR agonist); siLC, small intestine lumen content; cLC, colon
333 lumen content. *P < .05, **P < .01, ***P < .001, One-way ANOVA with Dunett's correction for
334 multiple comparisons. NS, not significant. **(f)** Mouse (m)CAR:human (h)RXRα ligand-binding domain
335 (LBD) heterodimer activation ($\pm$ SEM; n=3), by TR-FRET, +/- TC or 9-*cis* retinoic acid (RA, hRXRα
336 agonist). Numbers indicate EC_{50}'s; representative of 5 experiments. **(g)** Mean mCAR:hRXRα LBD
337 heterodimer activation ($\pm$ SEM; n = 3), by TR-FRET, +/- mouse tissue extracts. (*L-R*): 0%; 0.01%,
338 0.1%,, 1% extract. Incorporates data from 3 experiments. *P < .05, ****P < .0001, one-way ANOVA
339 with Tukey's correction for multiple comparisons. NS, not significant.
340
341 **Fig. 3. CAR promotes T cell IL-10 expression. (a)** Type 1 regulatory (Tr1) cell-signature enrichment
342 among genes reduced in CAR-deficient (B6.*Nr1i3*$^{-/-}$) *vs*. wild type (B6) small intestine lamina propria
343 (siLP) T effector (Teff) cells. NES, normalized enrichment score. **(b)** Enrichment of T cell lineage-
344 specific genes (x-axis; see methods) within genes differentially expressed between wild type and CAR-
345 deficient Teff cells per tissue (y-axis). **(c)** *Il10* expression, by RNA-seq (n = 3; see Fig. 2a), in wild
346 type or CAR-deficient spleen, siLP, or cLP Teff cells. Paired two-tailed student's t test P values are
347 shown. **(d)** *Left*, mixed T cell transfer approach to analyze CAR-dependent *Il10*-reporter (Thy1.1[24])
348 expression in Teff cells. *Right*, *ex vivo* Thy1.1 (*Il10*) staining, in wild type or CAR-deficient Teff cells
349 as above. Representative of 4 mice in 2-independent experiments. **(e)** Mean Thy1.1 (*Il10*)-expressing
350 wild type or CAR-deficient Teff cell percentages (n = 4; $\pm$ SEM) as in (d). *P < .05, **P < .01, One-
351 way ANOVA with Tukey's correction for multiple comparisons. **(f)** Mean relative *Il10* expression ($\pm$
352 SEM; n = 3), by qPCR, in *ex vivo*-isolated wild type or CAR-deficient Teff cells stimulated +/- mouse
353 tissue extracts. Veh, vehicle; TC, TCPOBOP (CAR agonist); siLC, small intestine lumen content; cLC,
354 colon lumen content. *P < .05, **P < .01, One-way ANOVA with Dunett's correction for multiple
355 comparisons. NS, not significant. **(g)** Box and violin plot of CAR/*Nr1i3* expression relative to $CD4^+$
356 naïve T cells (Tnaive; n = 2), by qPCR, in *in vitro*-polarized wild type effector or regulatory subsets.
357 npTh17, non-pathogenic Th17 cells; pTh17, pathogenic Th17 cells. **(h)** Intracellular IL-10/IFNγ
358 staining in wild type or CAR-deficient Tr1-like cells. Representative of 5 experiments; numbers
359 indicate percentages. **(i)** Mean percentages (n = 5; $\pm$ SEM) of IL-10^+ Tr1-like cells as in (h). **P <
360 .01, paired two-tailed student's t test.
361

bioRxiv preprint doi: https://doi.org/10.1101/2020.07.30.229864; this version posted January 4, 2021. The copyright holder for this preprint (which was not certified by peer review) is the author/funder, who has granted bioRxiv a license to display the preprint in perpetuity. It is made available under aCC-BY-NC-ND 4.0 International license.

362 **Fig. 4. CAR activation in T cells suppresses bile acid-driven ileitis. (a)** Mean relative *Abcb1a*,
363 *Cyp2b10* or *Il10* expression (± SEM; n = 3), by qPCR, in wild type (B6) or CAR-deficient (B6.*Nr1i3*$^{-/-}$
364) T effector (Teff) cells from spleens of co-transferred B6.*Rag1*$^{-/-}$ mice 72 hr after TC (TCPOBOP;
365 CAR agonist) or vehicle treatment. Expression in cells from TC-treated mice is shown relative to that
366 from vehicle-treated animals; data points are from 3-independent experiments. *P < .05, paired two-
367 tail student's t test. **(b)** Mean weight loss (± SEM) in co-housed *Rag2*$^{-/-}$ mice receiving wild-type naïve
368 T cells and maintained on a CA-supplemented diet with (red; n = 18) or without (blue; n = 16) weekly
369 TC treatment. CA-fed *Rag2*$^{-/-}$ mice without T cell transfer (no T cells; grey; n =10), and *Rag2*$^{-/-}$ mice
370 receiving wild type T cells but left on control chow diet and treated with vehicle (black, n = 17) are
371 also shown. Weights are relative to the start of TC treatment (3-weeks post-T cell transfer). *P < .05,
372 **P < .01, Two-way ANOVA. **(c)** *Top,* H&E-stained colons or terminal ilea from *Rag2*$^{-/-}$ mice
373 receiving wild type T cells and fed and treated as in (b). Analyzed at week-4 post-TC treatment;
374 representative of 3-4 mice/group. *Bottom,* mean histology scores (± SEM) for colons (n = 3-4) or
375 terminal ilea (n = 3) as in (c). *P < .05, one-way ANOVA with Tukey's correction for multiple
376 comparisons. NS, not significant. **(d)** Model of CAR-dependent T cell regulation in the small intestine.
377 CYPs, cytochrome P450 enzymes.

bioRxiv preprint doi: https://doi.org/10.1101/2020.07.30.229864; this version posted January 4, 2021. The copyright holder for this preprint (which was not certified by peer review) is the author/funder, who has granted bioRxiv a license to display the preprint in perpetuity. It is made available under aCC-BY-NC-ND 4.0 International license.

378 **Methods**

379 **Mice.** C57BL/6 (B6)-derived wild type (Stock No: 000664), CD45.1 (Stock No: 002014), *Rag1*$^{-/-}$
380 (Stock No: 002216), *Rag2*$^{-/-}$ (Stock No: 008449) and *Il10*$^{-/-}$ (Stock No: 002251) mice were purchased
381 from The Jackson Laboratory. Wild type FVB/N mice were purchased from Taconic. B6-derived
382 *Nr1i2*$^{-/-}$, *Nr1i3*$^{-/-}$ and *Nri12*$^{-/-}$*Nr1i3*$^{-/-}$ mice were provided by D. Moore (Baylor College of Medicine,
383 BCM). FVB-derived *Rag1*$^{-/-}$ mice were a gift of Dr. Allan Bieber (Mayo Clinic, Rochester, MN). B6-
384 derived BAC *Il10*-Thy1.1 transgenic reporter (10BiT) mice were provided by C. Weaver (University
385 of Alabama-Birmingham, UAB) and have been described previously[24]. B6-derived *Rag1*$^{-/-}$ mice were
386 crossed with *Slc10a2*$^{-/-}$ mice (gift of Dr. Paul Dawson, Emory University) in the Sundrud lab to
387 generate *Rag1*$^{-/-}$ mice lacking the Asbt transporter as in[4]. Lumen contents (colon, small intestine) were
388 harvested (see below) from specific pathogen-free (SPF) or germ-free wild type B6 mice housed at the
389 University of Alabama-Birmingham (UAB; courtesy of Dr. Weaver). All breeding and experimental
390 use of animals was conducted in accordance with protocols approved by IACUC committees at Scripps
391 Florida, BCM or UAB.

392

393 **Human blood samples.** Human blood samples were collected and analyzed in accordance with
394 protocols approved by Institutional Review Boards at Scripps Florida and OneBlood (Orlando,
395 Florida). Blood was obtained following informed written consent, and consenting volunteers willingly
396 shared clinical history and demographic information prior to phlebotomy. Institutional Review Boards
397 at OneBlood and Scripps Florida approved all procedures and forms used in obtaining informed
398 consent, and all documentation for consenting volunteers is stored at OneBlood.

399

400 **CD4^{+} T cell isolation and culture.** Purified CD4^{+}CD25^{-} T cells were magnetically isolated from
401 spleen and peripheral lymph node mononuclear cells using an EasySep magnetic T cell negative
402 isolation kit (Stem Cell Technologies, Inc.) with addition of a biotin anti-mouse CD25 antibody (0.5
403 μg/mL; BioLegend). Magnetically-enriched CD4^{+} T cells were cultured in (DMEM) supplemented
404 with 10% heat-inactivated fetal bovine serum (BioFluids), 2mM L-glutamine (Gibco), 50uM 2-
405 mercaptoethanol (Amresco), 1% MEM vitamin solution (Gibco), 1% MEM non-essential amino acids
406 solution (Gibco), 1% Sodium Pyruvate(Gibco), 1% Arg/Asp/Folic acid (Gibco), 1% HEPES (Gibco),
407 0.1% gentamicin (Gibco) and 100u/ml Pen-Strep (Gibco). For *Rag1*$^{-/-}$ transfer experiments,
408 magnetically enriched CD4^{+}CD25^{-} T cells were FACS-sorted to obtain pure naïve T cells
409 (CD3^{+}CD4^{+}CD25^{-}CD62L^{hi}CD44^{lo}). For *ex vivo* isolation of mononuclear cells from tissues of T cell-

bioRxiv preprint doi: https://doi.org/10.1101/2020.07.30.229864; this version posted January 4, 2021. The copyright holder for this preprint (which was not certified by peer review) is the author/funder, who has granted bioRxiv a license to display the preprint in perpetuity. It is made available under aCC-BY-NC-ND 4.0 International license.

410 reconstituted Rag-deficient mice, single cell suspensions were prepared from spleen, peripheral lymph
411 nodes, or mesenteric lymph nodes (MLN) by mechanical disruption passing through 70 μm nylon
412 filters (BD Biosciences). For intestinal tissues, small intestines and colons were removed, rinsed
413 thoroughly with PBS to remove the fecal contents, and opened longitudinally. Tissues were incubated
414 for 30 minutes at room temperature in DMEM media without phenol red (Genesee Scientific) plus
415 0.15% DTT (Sigma-Aldrich) to eliminate mucus layer. After washing with media, intestines were
416 incubated for 30 minutes at room temperature in media containing 1 mM EDTA (Amresco) to remove
417 the epithelium. Intestinal tissue was digested in media containing 0.25 mg/mL liberase TL (Roche) and
418 10 U/mL RNase-free DNaseI (Roche) for 15-35 minutes at 37 ^{o}C. Lymphocyte fractions were obtained
419 by 70/30% Percoll density gradient centrifugation (Sigma-Aldrich). Mononuclear cells were washed in
420 complete T cell media and resuspended for downstream FACS analysis or sorting.

421 *Naïve CD4^{+} T cell activation and polarization*: magnetically enriched CD4^{+}CD25^{-} T cells were seeded
422 (at 4x10^{5} cells/cm^{2} and 1x10^{6} cells/mL) in 96- or 24-well flat bottom plates pre-coated for 2 hr at 37 ^{o}C
423 with goat-anti-hamster whole IgG (50 μg/mL; Invitrogen). Activation was induced by adding hamster-
424 anti-mouse CD3ε (0.3 or 1 μg/mL; BioLegend) and hamster-anti-mouse CD28 (0.25 or 0.5 μg/mL;
425 BioXcell). After 48 hr, cells were removed from coated wells and re-cultured at 1x10^{6} cells/mL in
426 media with or without 10 U/mL recombinant human IL-2 (rhIL-2) (NIH Biorepository), depending on
427 the experiment (see below). For polarization studies, cells were activated in the presence of the
428 following sets of cytokines and/or neutralizing antibodies (all from R&D Systems): Th0—media alone;
429 Th1—recombinant human (rh)IL-12 (5 ng/mL) plus anti-mouse IL-4 (5 μg/mL); Th2—rhIL-4 (10
430 ng/mL) plus anti-mouse IFNγ (5 μg/mL); non-pathogenic (np)Th17—recombinant mouse (rm)IL-6 (40
431 ng/mL) plus rhTGFβ1 (1 ng/mL), anti-mouse IFNγ (5 μg/mL) and anti-mouse IL-4 (5 μg/mL);
432 pathogenic (p)Th17— rmIL-6 (40 ng/mL) plus rhTGFβ1 (1 ng/mL), rhIL-23 (10 ng/mL) anti-mouse
433 IFNγ (5 μg/mL) and anti-mouse IL-4 (5 μg/mL); induced T regulatory (i)Treg—rhTGFβ1 (5 ng/mL)
434 plus rhIL-2 (10 U/mL), anti-mouse IFNγ (5 μg/mL) and anti-mouse IL-4 (5 μg/mL). For Tr1 cultures,
435 cells were activated in the presence of rhIL-27 (100 ng/mL) and/or dexamethasone (100 nM; Sigma-
436 Aldrich). Cytokine, antibodies and/or Dex were added at the time of activation (day 0), and re-added to
437 expansion media between days 2-4 of culture. Cells were analyzed for intracellular expression of
438 transcription factors and/or cytokines, to confirm polarization, on day 4 after re-stimulation with
439 phorbol 12-myrisate 13-acetate (PMA; 10nM; Life Technologies) and ionomycin (1uM; Sigma-
440 Aldrich) for 3-4 hr in the presence of brefeldin A (BFA; 10ug/mL; Life Technologies).

bioRxiv preprint doi: https://doi.org/10.1101/2020.07.30.229864; this version posted January 4, 2021. The copyright holder for this preprint (which was not certified by peer review) is the author/funder, who has granted bioRxiv a license to display the preprint in perpetuity. It is made available under aCC-BY-NC-ND 4.0 International license.

441 *Ex vivo-stimulation of FACS-sorted effector/memory (Teff) cells from reconstituted Rag1$^{-/-}$ mice*:
442 30,000 CD45.1 (wild type) or CD45.2 (*Nr1i3*$^{-/-}$) cells—FACS-purified from spleens of B6.*Rag1*$^{-/-}$ 2-3
443 weeks post naïve T cell transfer—were activated in round-bottom 96-well plates with mouse anti-
444 CD3/anti-CD28 T cell expander beads (1 bead/cell; Life Technologies) in complete media containing
445 10 U/mL recombinant human (rh) IL-2 for 24 hr in the presence or absence of synthetic or endogenous
446 CAR agonists (see 'compound and tissue extracts' below).
447
448 **Retroviral plasmids and transductions.** shRNAmirs against mouse nuclear receptors were purchased
449 (TransOMIC) or custom synthesized using the shERWOOD algorithm[41]. For cloning into an ametrine-
450 expressing murine retroviral vector (LMPd) containing the enhanced miR-30 cassette[42,43], shRNAmirs
451 were PCR amplified using forward (5′-AGAAGGCTCGAGAAGGTATATTGC-3′) and reverse (5′-
452 GCTCGAATTCTAGCCCCTTGAAGTC CGAGG-3′) primers containing XhoI and EcoR1 restriction
453 sites, respectively. All retroviral constructs were confirmed by sequencing prior to use in cell culture
454 experiments. Retroviral particles were produced by transfection of Platinum E (PLAT-E) cells with the
455 TransIT-LT1 transfection reagent (Mirus) in Opti-MEM I reduced serum medium. Viral supernatants
456 containing 10 μg/mL polybrene were used to transduce CD4^{+}CD25^{-} T cells 24 hr post-activation (anti-
457 CD3/anti-CD28; as above). Transductions were enhanced by centrifugation at 2000 rpm for 1 hr at
458 room temperature, and incubation at 37 ^{o}C until 48 hr post-activation. Transduced cells were expanded
459 in complete media containing 10 U/mL rhIL-2.
460
461 **Cell lines.** PLAT-E cells, derived from the HEK-293 human embryonic kidney fibroblasts and
462 engineered for improved retroviral packaging efficiency, were provided by M. Pipkin (Scripps
463 Florida). All cell lines were tested to be mycoplasma free, and cultured in DMEM plus 10% FBS, 2
464 mM L-glutamine, 50 uM 2-mercaptoethanol, 1% HEPES, 0.1% gentamicin and 100u/ml Pen-Strep.
465
466 **T cell transfer colitis.** For experiments using B6-derived wild-type or CAR-deficient (*Nr1i3*$^{-/-}$) T cells,
467 0.5 x 10^{6} FACS-sorted naïve T cells (sorted as CD4^{+}CD25^{-}CD62L^{hi}CD44^{lo} at Scripps Florida;
468 CD4^{+}CD45RB^{hi} at BCM) were injected intraperitoneally (i.p.) into syngeneic *Rag1*$^{-/-}$ (at Scripps
469 Florida) or *Rag2*$^{-/-}$ (at BCM) recipients and analyzed between 2-6 weeks post-transfer. For mixed
470 congenic T cell transfers, FACS-purified naïve T cells (CD4^{+}CD25^{-}CD62L^{hi}CD44^{lo}) from CD45.1
471 wild type and CD45.2 CAR-deficient (*Nr1i3*$^{-/-}$), PXR-deficient (*Nr1i2*$^{-/-}$), CAR- and PXR-deficient
472 (*Nri12*$^{-/-}$*Nr1i3*$^{-/-}$) or *Il10*$^{-/-}$ mice were mixed in a 1:1: ratio and transferred together (0.5 x 10^{6} total

bioRxiv preprint doi: https://doi.org/10.1101/2020.07.30.229864; this version posted January 4, 2021. The copyright holder for this preprint (which was not certified by peer review) is the author/funder, who has granted bioRxiv a license to display the preprint in perpetuity. It is made available under aCC-BY-NC-ND 4.0 International license.

473 cells). For transfers of shRNAmir-expressing T cells, magnetically enriched CD4^{+}CD25^{-} T cells from
474 FVB/N (FVB) wild-type mice, activated and transduced as above, were expanded until day 5 in media
475 containing rhIL-2 and transferred into syngeneic *Rag1*$^{-/-}$ mice (0.5 x 10^{6} total cells). All *Rag1*$^{-/-}$
476 recipients were weighed immediately prior to T cell transfer to determine baseline weight, and then
477 weighed twice weekly after T cell transfer for the duration of the experiment. Mouse chow diets
478 containing 2% Cholestyramine (CME) (Sigma-Aldrich) or 0.2% Cholic Acid (CA) (Sigma-Aldrich)
479 and control diets were custom made (Teklad Envigo, Madison, WI) and fed to mice as follows: CME-
480 supplemented diets were started 3 weeks after T cell transfer and continued for 3 weeks; cholic acid
481 diet was started within 3 days post-T cell transfer and continued for 6 weeks (or until mice died).
482 TCPOBOP (TC; Sigma-Aldrich) was initially reconstituted in sterile DMSO, stored at -20 ^{o}C, and
483 diluted in sterile saline and sonicated immediately prior to injections. 3 mg/kg TC was injected intra-
484 peritoneal (i.p.) weekly as indicated. Transferred *Rag1*$^{-/-}$ or *Rag2*$^{-/-}$ mice were euthanized upon losing
485 20% of pre-transfer baseline weight. All *Rag*$^{-/-}$ mice receiving different donor T cell genotypes were
486 co-housed to normalize microflora exposure.
487
488 **Anti-CD3-induced intestinal injury.** Wild-type (B6) or CAR-deficient (B6.*Nr1i3*$^{-/-}$) mice were
489 injected i.p. with 15 ug of soluble, Ultra-LEAF purified anti-CD3 (clone: 145-2C11) or IgG isotype
490 control (clone: HTK888) (BioLegend) twice over 48 hr. Animals were euthanized, and T cells
491 analyzed 4 hr after the second injection.
492
493 **Histology.** Colon (proximal, distal) or small intestine (proximal, mid, distal/ileum) sections (~ 1 cm)
494 were cut from euthanized *Rag1*$^{-/-}$ or *Rag2*$^{-/-}$ mice 6 weeks post-T cell transfer. In some experiments, 10
495 cm segments of distal small intestine and whole colon were dissected from mice and fixed intact. All
496 tissues were fixed in 10% neutral buffered formalin, embedded into paraffin blocks, cut for slides at 4-
497 5 microns, and stained with hematoxylin and eosin (H&E). H&E-stained sections were analyzed and
498 scored blindly by a pathologist with GI expertise using an Olympus BX41 microscope and imaged
499 using an Olympus DP71 camera. Colons and ilea were histologically graded for inflammation severity
500 using a combination of previously-reported grading models published by Kim, et al.[31] and by Berg et
501 al.[32]. The scheme published by Kim, et al grades 5 different descriptors which include crypt
502 architecture (normal, 0 - severe crypt distortion with loss of entire crypts, 3), degree of inflammatory
503 cell infiltration (normal, 0 – dense inflammatory infiltrate, 3), muscle thickening (base of crypt sits on
504 the muscularis mucosae, 0 - marked muscle thickening present, 3), goblet cell depletion (absent, 0-

bioRxiv preprint doi: https://doi.org/10.1101/2020.07.30.229864; this version posted January 4, 2021. The copyright holder for this preprint (which was not certified by peer review) is the author/funder, who has granted bioRxiv a license to display the preprint in perpetuity. It is made available under aCC-BY-NC-ND 4.0 International license.

505 present, 1) and crypt abscess (absent, 0- present, 1). The histological damage score is the sum of each
506 individual score.
507
508 **Flow cytometry.** Cell surface and intracellular FACS stains were performed at 4 °C for 30 minutes,
509 washed with phosphate buffered saline (PBS) and acquired on a flow cytometer. Analysis of Rh123
510 efflux was performed as in[4]. Background Rh123 efflux was determined by the addition of the MDR1
511 antagonist, elacridar (10 nM), to Rh123-labelled cells prior to the 37 °C efflux step. Anti-mouse
512 antibodies used for FACS analysis included: Alexa Fluor 700 anti-CD45, APC anti-CD45.1, BV711
513 anti-CD4, BV510 anti-CD25, BV650 anti-CD3, Percp-Cy5.5 anti-CD62L, PE-CY7 anti-CD44, BV605
514 anti-CD62L, PE anti-α4β7, Alexa Fluor700 anti-CD4, FITC anti-CD44, BV421 anti-CD44, e450 anti
515 FOXP3, BV605 anti-TNF, Percp-Cy5.5 anti-Il-17a, BV711 anti-INFγ, PE anti-Il-4, PE-CY7 anti-IL-
516 10, PE anti-Thy1.1, FITC anti-CD3, Percp-Cy5.5 anti-Thy1.1, PE anti-CD3, PE anti-TCRβ, APC anti-
517 INFg, FITC anti-CD45.2, PE anti-α4β7 (from BioLegend); and BUV395 anti-CD3, PE-CF594 anti-
518 CD25, FITC anti-Ki-67, PE-CF594 anti-RORγt, FITC anti-CD4, PE anti-CD45RB (from BD). Anti-
519 human antibodies used for FACS analysis included: APC anti-CD3, PE anti-CD4, PE-Cy7 anti-
520 CD45RO, BV711 anti-CD49a (integrin α4), APC-Fire 750 anti-integrin β7, BV421 anti-CCR9, and
521 Percp-Cy5.5 anti-CCR7, BV605 anti-CCR2, PE anti-CRTH2, PE anti-CCR10, PE-Cy7 anti-CCR4,
522 Percp-Cy5.5 anti-CXCR3, APC anti-CCR6, BV605 anti-CD4, PE-CF594 anti-CD25 (from BD). Vital
523 dyes include: fixable viability eFluor® 506, eFluor® 660 and eFluor® 780 (all from eBioscience).
524 Rh123 and elacridar were purchased from Sigma-Aldrich. All FACS data was acquired on LSRII or
525 FACSCanto II instruments (BD), and analyzed using FlowJo 9 or FlowJo 10 software (TreeStar, Inc.).
526 (We're probably missing a bunch).
527
528 **Cell sorting.** Cells stained with cell-surface antibodies, as above, were passed through 70 μm nylon
529 filters, resuspended in PBS plus 1% serum, and sorted on a FACS AriaII machine (BD Biosciences).
530 Sorted cells were collected in serum-coated tubes containing PBS plus 50% serum. Gates used to sort
531 MDR1+/- T cells, based on Rh123 efflux, were set using background Rh123 efflux in elacridar-treated
532 cells. For human T cell sorts, Peripheral blood mononuclear cells (PBMC) were isolated using Ficoll-
533 Plaque PLUS (GE Healthcare) from 25 mL of enriched buffy coats (OneBlood). $CD4^+$ T cells were
534 enriched using the Human total CD4 T cell Negative Isolation kit (EasySep), followed by enrichment
535 of either effector/memory T cells (Human Memory CD4 T cell Enrichment kit; EasySep) or Treg cells
536 (Human $CD4^+CD127^{lo}CD49d^-$ Treg Enrichment Kit; EasySep) (all from StemCell Technologies).

bioRxiv preprint doi: https://doi.org/10.1101/2020.07.30.229864; this version posted January 4, 2021. The copyright holder for this preprint (which was not certified by peer review) is the author/funder, who has granted bioRxiv a license to display the preprint in perpetuity. It is made available under aCC-BY-NC-ND 4.0 International license.

537 Enriched cells were stained with anti-human FACS antibodies (listed above) for 20 minutes on ice.
538 Stained cells were filtered through sterile 40 uM mesh filters and re-suspended in PBS with 5% FBS
539 and 0.1% DNase. In cases where RNA was isolated after sorting, 100,000 cells were sorted into 200
540 uL PBS with 1 uM DTT and 5 uL RNase Inhibitor Cocktail (Takara); for *ex vivo* culture experiments,
541 0.4-1.2 $x10^6$ cells were sorted into complete T cell media.
542

543 **Pooled *in vivo* shRNAmir screen.** Two independent pooled screens were performed. Briefly, PLAT-E
544 cells were cultured in 96 well plates with 5 x 10^4 per well in 100uL complete medium and transfected
545 as described above. Magnetically enriched $CD4^+CD25^-$ T cells from spleens of 7- to 8-week old female
546 FVB/N (FVB) mice were activated with anti-CD3 and anti-CD28 in 96 well plates and transduced 24
547 hr post-activation. Transduction efficiency of each individual shRNA was determined on day 4;
548 transduced cells were pooled and FACS-sorted for $ametrine^+$ on day 5 and adoptively transferred (i. p.)
549 into 10 FVB.*Rag1*$^{-/-}$ mice. An aliquot of sorted cells was saved for genomic DNA isolation and used
550 for input reference. Six weeks post-transfer, live (viability dye^-) transduced ($ametrine^+$) $Rh123^{hi}$
551 ($MDR1^-$) or $Rh123^{lo}$ ($MDR1^+$) effector/memory T cells (Teff; $CD4^+CD25^-CD62L^{lo}CD44^{hi}$) were
552 FACS-sorted from the spleen or small intestine lamina propria of FVB.*Rag1*$^{-/-}$ recipients. High quality
553 genomic DNA was isolated using PureLink® Genomic DNA Mini Kit (Invitrogen) and 100 ng of
554 DNA was used for library preparation. gDNA derived from transduced and sorted T cells were
555 quantified with Qubit DNA assay. 75ng of gDNA were used as template in duplicate reactions to add
556 the Ion adapter sequences and barcodes. Based on previous data, 28 cycles of PCRs were used to
557 amplify the libraries using primers with Ion P1 miR30 loop sequence (5'-
558 CCTCTCTATGGGCAGTCGGTGATTACATCTGTGGCTTC-ACTA-3') and Ion A miR-30 (5'-
559 CCATCTCATCCCTGCGTGTCTCCGACTCAGXXXXXXXXXX-
560 GCTCGAGAAGGTATATTGCT-3') sequences. The miR-30 loop (PI) and miR-30 (A) annealing
561 sequences are underlined. The IonXpress 10 nt barcode is depicted with a string of X's. Sequencing
562 libraries were purified with 1.6X Ampure XP beads (Beckman Coulter), quantified with Qubit DNA
563 HS assay (Invitrogen), and visualized on the Agilent 2100 Bioanalyzer (Agilent Technologies, Inc.).
564 Individually-barcoded libraries were pooled at equimolar ratios and templated on to Ion spheres at 50
565 pM loading concentration using the Ion Chef (Life Technologies) with the Ion PI IC 200 kit. The
566 templated Ion spheres (ISPs) were quantified using AlexaFluor sequence-specific probes provided in
567 the Ion Spehere quality control kit (Life Technologies). The percent templated ISPs within 10-20%
568 were taken forward to loading on the Ion PI V2 chips and then run on the Ion Proton with 200 bp
569 reads. Libraries were sequenced using the Ion Torrent technology from Life Technologies following

bioRxiv preprint doi: https://doi.org/10.1101/2020.07.30.229864; this version posted January 4, 2021. The copyright holder for this preprint (which was not certified by peer review) is the author/funder, who has granted bioRxiv a license to display the preprint in perpetuity. It is made available under aCC-BY-NC-ND 4.0 International license.

570 the manufacturer's instructions. Sequencing reads were aligned to the reference library using BLAST
571 with default settings and raw counts were normalized with DESeq2. Normalized reads of shRNAmirs
572 displaying $\leq$ 10-fold change between input and *ex vivo* spleen samples were considered for
573 downstream analysis. The relative enrichment or depletion of shRNAmirs was determined using
574 median $\log_2$ fold-changes in shRNAmir abundances in MDR1^{hi} *vs*. MDR1^{lo} Teff cells. Median values
575 for each gene target were calculated based on mean shRNAmir abundances determined in 2-
576 indpeendent screens, each using cells recovered from pools of 10 spleens and siLP of transferred
577 FVB.*Rag1*$^{-/-}$ mice.
578
579 **Compounds and tissue extracts.** 10 or 20 uM 1,4-Bis-[2-(3,5-dichloropyridyloxy)]benzene, 3,3′,5,5′-
580 Tetrachloro-1,4-bis(pyridyloxy) benzene (TC), 10 uM 5α-Androstan-3β-ol (And), 10 uM 5-Pregnen-
581 3β-ol-20-one-16α-carbonitrile (PCN) (all from Sigma-Aldrich)—or serum, bile (from gallbladder),
582 sterile soluble small intestine lumen content (siLC), or sterile soluble colon lumen content (cLC) from
583 wild type (B6) mice—were added to mouse naïve or effector/memory (Teff) cells stimulated with anti-
584 CD3/anti-CD28 antibodies as above. For preparation of mouse tissue extracts, mouse small intestinal
585 lumen content (siLC) or colon lumen content (cLC) was extracted from whole tissue into a sterile tube.
586 Contents were weighed, diluted with an equal volume of sterile PBS, vortexed vigorously for 30 sec,
587 and then supernatants were collected after sequential centrifugation steps: (*i*) 10 min at 930 x *g*; and
588 (*ii*) 10 min at 16 x *g*. Cleared supernatants were finally sterile-filtered using 0.22 µm filters and
589 aliquots were frozen at -20° C. Serum was collected in EDTA coated tubes and centrifuged for 5 min at
590 2.4 x *g*. Due to small sample size, serum and gallbladder bile were used directly without filter
591 sterilization after harvesting. Equal volumes of sterile vehicles (DMSO for TC, And; ethanol for PCN;
592 PBS for sterile mouse content) served as negative controls. For human T cell culture experiments,
593 healthy adult donor PBMC were FACS-sorted for the following subsets: (*i*) naïve CD4^{+} T cells
594 (CD4^{+}CD25^{-}CD45RO^{-}CCR7^{hi}); (*ii*) Treg cells (CD4^{+}CD25^{hi}); (*iii*) α4^{-}CCR9^{-} effector/memory cells
595 (Teff; CD4^{+}CD25^{-}CD45RO^{+}); and (*iv*) α4^{+}CCR9^{+} effector/memory cells (Teff; CD4^{+}CD25^{-}
596 CD45RO^{+}). Note that all α4^{-}CCR9^{-} Teff cells are integrin β7^{-}and all α4^{+}CCR9^{+} Teff cells are integrin
597 β7^{+}. For all subsets, 30,000 purified cells were stimulated in round-bottom 96-well plates with human
598 anti-CD3/anti-CD28 T cell expander beads (1 bead/cell; ThermoFisher) in complete media containing
599 10 U/mL rhIL-2 with or without 10 or 20 uM 6-(4-Chlorophenyl)imidazo[2,1-b][1,3]thiazole-5-
600 carbaldehyde O-(3,4-dichlorobenzyl)oxime (CITCO) (Sigma-Aldrich); an equal volume of DMSO
601 served as the negative control.

bioRxiv preprint doi: https://doi.org/10.1101/2020.07.30.229864; this version posted January 4, 2021. The copyright holder for this preprint (which was not certified by peer review) is the author/funder, who has granted bioRxiv a license to display the preprint in perpetuity. It is made available under aCC-BY-NC-ND 4.0 International license.

602

603 **qPCR.** RNA was isolated from cultured or ex vivo-isolated cells using RNeasy Mini columns with on-
604 column DNase treatment (Qiagen); RNA was used to synthesize cDNA via a high capacity cDNA
605 reverse transcription kit (Life Technologies). Taqman qPCR was performed on a StepOnePlus real
606 time PCR instrument (Life Technologies/Applied Biosystems) using commercial Taqman
607 primer/probe sets (Life Technologies). Probes for mouse genes included: *Abcb1a* (Mm00607939_s1),
608 *Nr1i3* (Mm01283981_g1), *Cyp2b10* (Mm01972453_s1), *Il10* (Mm01288386_m1) and *Actin b*
609 *(Mm00607939_s1)*; probes for human genes included: *NR1I3* (Hs00901571_m1), *ABCB1*
610 (Hs00184500_m1), *CYP2B6* (Hs04183483), *IL10* (Hs00961622_m1), and *ACTIN B* (Hs0160665_g1).
611

612 **Bioinformatics.** *ChIP-seq*: Raw sequencing reads for CAR were downloaded from Gene Expression
613 Omnibus (GSE112199)[17], aligned to USC mm10 with Bowtie2[33] and analyzed with MACS[34] using
614 base settings. Biological replicate reads files were merged into a single file and bigwig files were
615 generated and visualized with Integrated Genome Viewer (IGV)[35]. Peaks were filtered to remove reads
616 with alternative annotations, mitochondrial DNA, or blacklist regions in R using GenomeInfoDb and
617 GenomicRanges package.
618 *RNA-seq*: Next-generation RNA-sequencing (RNA-seq) was performed on FACS-sorted B6 wild type
619 and CAR-deficient effector/memory T cells (Teff cells: viability dye$^-$CD45$^+$CD3$^+$CD4$^+$CD25$^-$CD44^{hi})
620 from spleen, small intestinal lamina propria, and colon lamina propria of *Rag1*$^{-/-}$ mice injected 3-weeks
621 prior with congenic mixtures of CD45.1 wild type and CD45.2 *Nr1i3*$^{-/-}$ naïve T cells, approximately
622 500 sorted cells were processed directly to generate cDNA using the Clontech SMART-Seq v4 Ultra
623 Low Input Kit (Clontech, Inc.) on three biologically-independent replicates. The generated cDNA was
624 size selected using beads to enrich for fragments > 400 bp. The enriched cDNA was converted to
625 Illumina-compatible libraries using the NEBNext Ultra II DNA kit (New England Biolabs, Inc.) using
626 1ng input. Final libraries were validated on the Agilent 2100 bioanalyzer DNA chips and quantified on
627 the Qubit 2.0 fluorometer (Invitrogen, Life Technologies). Barcoded libraries were pooled at
628 equimolar ratios and sequenced using single-end 75 bp reads on a NextSeq 500 instrument (Illumina).
629 Raw sequencing reads (fastq files) were mapped to the mm10 transcriptome and transcript abundance
630 in terms of Transcripts Per Million (TPM) were quantified using Salmon[48]. PCA was performed and
631 projected in R-studio. Differentially expressed genes (DEG) were determined using DESeq2 ($P < .05$)
632 for CAR-deficient (B6.*Nr1i3*$^{-/-}$) *vs.* wild type (B6) Teff cells from spleen (296 up; 285 down), siLP
633 (472 up; 523 down), or cLP (350 up; 228 down) and $\log_2$ fold-change was used as the ranking metric
634 to generate input ranked lists for gene set enrichment analysis (GSEA) (https://www.gsea-

bioRxiv preprint doi: https://doi.org/10.1101/2020.07.30.229864; this version posted January 4, 2021. The copyright holder for this preprint (which was not certified by peer review) is the author/funder, who has granted bioRxiv a license to display the preprint in perpetuity. It is made available under aCC-BY-NC-ND 4.0 International license.

635 msigdb.org/gsea/index.jsp); these genes were compared against both customized and curated gene sets
636 (the latter from the Molecular Signature Database (MSigDB)) for enrichment—quantified as
637 normalized enrichment score (NES)—and visualized using ggplot2 package in R. For GSEA summary
638 plots (Fig 2d, 3b; Extended Data Fig. 3b) circle sizes indicate significance (-$\log_{10}$ Padj values).
639 Red/blue coloring indicates enrichment within genes up/down, respectively, in CAR-deficient *vs*. wild
640 type cells, based on normalized enrichment score (NES). Differentially expressed genes of wild type
641 (B6) Teff cells from the spleen, siLP, or cLP determined by DESeq2 were used to generate tissue-
642 specific Teff gene sets: (*i*) up in B6 spleen Teff, genes selectively expressed in spleen *vs*. either siLP
643 or cLP wild type (B6) Teff cells; (*ii*) up in B6 siLP Teff, genes selectively expressed in siLP *vs*. either
644 spleen or cLP wild type (B6) Teff cells; and (*iii*) up in B6 cLP Teff, genes selectively expressed in cLP
645 *vs*. either spleen or siLP wild type (B6) Teff cells. RNA-seq data of pharmacological activation of
646 CAR or PXR in hepatocytes *in vivo* from mice treated with the CAR agonist, TCPOBOP (TC), the
647 PXR agonist, PCN, or vehicle (corn oil) (GSE104734)[16] were analyzed to generate the gene sets: Up in
648 Hep + TC, genes selectively induced by the CAR agonist, TCPOBOP (TC), compared with either
649 vehicle (corn oil) or the PXR agonist, PCN, in hepatocytes from mice treated with compounds *in vivo*;
650 and Up in Hep + PCN, genes selectively induced by the PXR agonist, PCN, compared with either
651 vehicle (corn oil) or the CAR agonist, TC, in hepatocytes from mice treated with compounds *in vivo*.
652 Differential gene expression of *in vitro*-differentiated Tr1 (GSE92940)[22] and Th17 cells (GSE21670)[36]
653 were determined using the Limma package in R (for microarray data)[37] to generate the gene sets: Tr1-
654 signature, genes selectively expressed in *in vitro*-differentiated Tr1 cells, compared with non-
655 polarizing conditions; and Th17-signature, genes selectively expressed in *in vitro*-differentiated Th17
656 cells, compared with non-polarizing conditions. Th1-signature, Th2-signature, induced (i)Treg-
657 signature (GSE14308)[38], or T follicular helper (Tfh)-signature (GSE21379)[39], genes selectively
658 induced in these *vs*. other T cell subsets, as curated on MSigDB (https://www.gsea-
659 msigdb.org/gsea/msigdb/index.jsp).
660
661 **TR-FRET co-regulator recruitment assay**. The DNA sequences encoding mouse (m)CAR ligand-
662 binding domain (LBD; residues 109 – 358) were amplified by PCR reaction and inserted into modified
663 pET24b vectors to produce pET24b-mCAR-LBD. pACYC-Duet1-RXR-LBD, an expression plasmid
664 for untagged human (h)RXRα LBD was provided by Dr. Eric Xu[40]. Purification of the mCAR-hRXRα
665 LBD heterodimer, as well as hRXRα homodimer, was achieved by nickel-affinity chromatography,
666 followed by size-exclusion chromatography in an Akta explorer FPLC (GE Healthcare). Briefly,

bioRxiv preprint doi: https://doi.org/10.1101/2020.07.30.229864; this version posted January 4, 2021. The copyright holder for this preprint (which was not certified by peer review) is the author/funder, who has granted bioRxiv a license to display the preprint in perpetuity. It is made available under aCC-BY-NC-ND 4.0 International license.

667 pET24b-mCAR-LBD and pACYC-Duet1-RXR-LBD were co-transformed into BL21 (DE3) for
668 mCAR-hRXRα heterodimer and pET46-RXRα-LBD was transformed into BL21 (DE3) for RXRα
669 homodimer. The cells were grown in 4 x 900 mL of LB media at 37 °C until the OD600 reached a
670 value of 0.6–0.7. Overexpression was induced by 0.3 mM of IPTG and the cells were grown further
671 for 22 hr at 18 °C. The harvested cells were resuspended in sonication buffer (500 mM NaCl, 10 mM
672 HEPES, 10 mM imidazole, pH 8.0, and 10% glycerol), sonicated on an ice-water bath for 20 min at 18
673 W output, and centrifuged for 25 min at 50,000 x g. The proteins were isolated from the sonicated
674 supernatant by applying to a 2 mL His Select column and eluted with linear gradient from 10 mM to
675 300 mM imidazole in sonication buffer. The elution fractions containing the proteins concentrated
676 while exchanging buffer to gel filtration buffer (300 mM NaCl, 20 mM HEPES, 1 mM DTT, 5 %
677 glycerol). The proteins were purified further by gel filtrations through a Superdex 200 26/60 column
678 (GE Healthcare) equilibrated with gel filtration buffer. Fractions containing the proteins were pooled
679 and concentrated to ~ 8 mg/mL each with 30 kDa cutoff ultrafiltration units (Millipore). Time-resolved
680 fluorescence resonance energy transfer (TR-FRET) assays were performed in low-volume black 384-
681 well plates (Greiner) using 23 μL final well volume. Each well contained the following components
682 in TR-FRET buffer (20 mM KH_2PO_4/K_2HPO_4, pH 8, 50 mM KCl, 5 mM TCEP, 0.005% Tween 20): 4
683 nM 6xHis-CAR/RXRα LBD heterodimer or 6xHis-RXRα/RXRα homodimer LBD, 1 nM
684 LanthaScreen Elite Tb-anti-His Antibody (ThermoFisher #PV5895), and 400 nM FITC-labeled PGC1α
685 peptide (residues 137–155, EAEEPSLLKKLLLAPANTQ, containing an N-terminal FITC label with a
686 six-carbon linker, synthesized by Lifetein). Pure ligand (TC, 9-*cis* RA) or tissue extracts (see above)
687 were prepared via serial dilution in vehicle (DMSO or PBS, respectively), and added to the wells along
688 with vehicle control. Plates were incubated at 25 °C for 1 hr and fluorescence was measured using a
689 BioTek Synergy Neo plate reader (Promega). The terbium (Tb) donor was excited at 340 nm, its
690 emission was monitored at 495 nm, and emission of the FITC acceptor was monitored at 520 nm. Data
691 were plotted as 520/340 nM rations using Prism software (GraphPad); TC data were fit to a sigmoidal
692 dose response curve equation.
693

694 **Statistical Analyses.** Statistical analyses were performed using Prism (GraphPad). *P* values were
695 determined by paired or unpaired student's *t* tests, Log-rank test, one-way ANOVA, and two-way
696 ANOVA analyses as appropriate and as listed throughout the Figure legends. Statistical significance of
697 differences (* P < 0.05, **P < 0.01, ***P < 0.001, ****P < 0.0001) are specified throughout the Figure
698 legends. Unless otherwise noted in legends, data are shown as mean values ± S.E.M.

bioRxiv preprint doi: https://doi.org/10.1101/2020.07.30.229864; this version posted January 4, 2021. The copyright holder for this preprint (which was not certified by peer review) is the author/funder, who has granted bioRxiv a license to display the preprint in perpetuity. It is made available under aCC-BY-NC-ND 4.0 International license.

699

700 **Reporting summary.** Further details regarding research design is available in the Nature Research
701 Reporting Summary linked to this paper.

702

703 **Data availability**

704 RNA-seq data for wild type and CAR-deficient effector $CD4^+$ T cells from spleen, small intestine
705 lamina propria or colon lamina propria of congenically co-transferred *Rag1*$^{-/-}$ mice, as well as from
706 human peripheral blood $\alpha4^+\beta7^+CCR9^+$ memory $CD4^+$ T cells stimulated *ex vivo* in the presence or
707 absence of the human CAR agonist, CITCO, are available on the NCBI Gene Expression Omnibus
708 (GEO) repository (accession ID: GSE149220).

709

710 **Code availability**

711 No proprietary code was written or used for data analyses in this study.

712

713 31 Kim, J. J., Shajib, M. S., Manocha, M. M. & Khan, W. I. Investigating intestinal inflammation
714 in DSS-induced model of IBD. *J Vis Exp*, doi:10.3791/3678 (2012).
715 32 Berg, D. J. *et al.* Enterocolitis and colon cancer in interleukin-10-deficient mice are associated
716 with aberrant cytokine production and CD4(+) TH1-like responses. *J Clin Invest* **98**, 1010-
717 1020, doi:10.1172/JCI118861 (1996).
718 33 Langmead, B. & Salzberg, S. L. Fast gapped-read alignment with Bowtie 2. *Nature methods* **9**,
719 357-359, doi:10.1038/nmeth.1923 (2012).
720 34 Zhang, Y. *et al.* Model-based analysis of ChIP-Seq (MACS). *Genome Biol* **9**, R137,
721 doi:10.1186/gb-2008-9-9-r137 (2008).
722 35 Robinson, J. T. *et al.* Integrative genomics viewer. *Nat Biotechnol* **29**, 24-26,
723 doi:10.1038/nbt.1754 (2011).
724 36 Durant, L. *et al.* Diverse targets of the transcription factor STAT3 contribute to T cell
725 pathogenicity and homeostasis. *Immunity* **32**, 605-615, doi:10.1016/j.immuni.2010.05.003
726 (2010).
727 37 Ritchie, M. E. *et al.* limma powers differential expression analyses for RNA-sequencing and
728 microarray studies. *Nucleic Acids Res* **43**, e47, doi:10.1093/nar/gkv007 (2015).

bioRxiv preprint doi: https://doi.org/10.1101/2020.07.30.229864; this version posted January 4, 2021. The copyright holder for this preprint (which was not certified by peer review) is the author/funder, who has granted bioRxiv a license to display the preprint in perpetuity. It is made available under aCC-BY-NC-ND 4.0 International license.

729 38 Wei, G. *et al.* Global mapping of H3K4me3 and H3K27me3 reveals specificity and plasticity in
730 lineage fate determination of differentiating CD4+ T cells. *Immunity* **30**, 155-167,
731 doi:10.1016/j.immuni.2008.12.009 (2009).
732 39 Yusuf, I. *et al.* Germinal center T follicular helper cell IL-4 production is dependent on
733 signaling lymphocytic activation molecule receptor (CD150). *Journal of immunology* **185**, 190-
734 202, doi:10.4049/jimmunol.0903505 (2010).
735 40 Suino, K. *et al.* The nuclear xenobiotic receptor CAR: structural determinants of constitutive
736 activation and heterodimerization. *Mol Cell* **16**, 893-905, doi:10.1016/j.molcel.2004.11.036
737 (2004).
738

739 **Acknowledgements** The authors thank Core Facility staff at Scripps Florida and Baylor College of
740 Medicine for technical support, and Drs. Paul Dawson and Anjana Rao for critical discussions. This
741 work was supported by Scripps Florida via the State of Florida (M.S.S.), the R.P. Doherty Jr.–Welch
742 Chair in Science Q□0022 at Baylor College of Medicine (D.D.M.), National Institute of Health grants
743 R21AI119728 (M.S.S.), R01AI118931-01 (M.S.S.), U19AI109976 (M.E.P), P01AI145815 (M.E.P.),
744 and a Senior Research Award from the Crohn's and Colitis Foundation (M.S.S.).
745

746 **Author contributions** Study design: M-L.C., X.H., H.W., J.S., H.P., B.F., L.A.S., D.J.K., A.R-P.,
747 D.A.S., C.T.W., M.E.P., D.D.M., and M.S.S. Data generation: M-L.C., X.H., H.W., C.H., Y.L., J.S.,
748 A.E., and S.A.M. Bioinformatics: M-L.C., G.W., A.R-P., and M.E.P. Manuscript: M-L.C., X.H., C.H.,
749 A.E., D.J.K., A. R-P., C.T.W., M.E.P., D.D.M., and M.S.S. Principal Investigators: L.A.S., D.J.K.,
750 A.R-P., D.A.S., C.T.W., M.E.P., D.D.M., and M.S.S.
751

752 **Competing interests** M.S.S. is a consultant to Sigilon Therapeutics and Sage Therapeutics.
753

754 **Additional information**
755 **Supplementary information** is available for this paper.
756 ***Correspondence and requests for materials** should be addressed to D.D.M. (Berkeley email address
757 pending) or M.S.S. (msundrud@scripps.edu).

bioRxiv preprint doi: https://doi.org/10.1101/2020.07.30.229864; this version posted January 4, 2021. The copyright holder for this preprint (which was not certified by peer review) is the author/funder, who has granted bioRxiv a license to display the preprint in perpetuity. It is made available under aCC-BY-NC-ND 4.0 International license.

758 **Extended Data Figure Legends**

759 **Extended Data Figure 1. Nuclear receptor-dependent regulation of effector T cell persistence**
760 **and MDR1 expression *in vivo*. (a)** *Top*, abundance of shRNAmirs in *ex vivo*-isolated spleen and *in*
761 *vitro*-transduced (input) Teff cells. shRNAmirs with $\leq$ 1 normalized read in both *ex vivo* spleen and
762 input Teff cell pools were considered 'poorly represented' (highlighted green). Well-represented
763 shRNAmirs displaying $\leq$ 10-fold change between *ex vivo* spleen and input Teff cell pools (between
764 blue lines) were considered for downstream analysis. *Bottom*, abundance of shRNAmirs, filtered for
765 minimal effects on *in vivo* Teff cell persistence, in *ex vivo*-isolated MDR1^{hi} (Rh123^{lo}) and MDR1^{lo}
766 (Rh123^{hi}) siLP Teff cells. **(b)** Log$_2$ fold-change in abundance ($\pm$ SEM) of shRNAmirs against *Cd19* (*n*
767 = 3), *Abcb1a* (*n* = 2), *Nr1i3* (*n* = 5), *Thra* (*n* = 6), and *Esrra* (*n* = 3) in FVB wild type Rh123^{lo}
768 (MDR1^{hi}) *vs*. Rh123^{hi} (MDR1^{lo}) effector/memory T cells (Teff; sorted as in Fig. 1a) recovered from
769 spleens or small intestine lamina propria (siLP) of transferred FVB.*Rag1*$^{-/-}$ mice. (a-b) Data
770 incorporates shRNAmir abundance, determined by DNA-seq, in 2-indpeendent screens using pooled
771 spleens and siLP from 10 transferred FVB.*Rag1*$^{-/-}$ mice per screen. **(c)** *Ex vivo* Rh123 efflux,
772 determined by flow cytometry, in FVB wild type Teff cells expressing a control shRNAmir against
773 CD8 (*shCD8a*) or 1 of 5-independent shRNAmirs against CAR (*shNr1i3*) isolated from spleens of
774 transferred FVB.*Rag1*$^{-/-}$ mice 6-weeks post-transfer. Rh123 efflux in transduced (Ametrine pos.; blue)
775 cells is overlaid with that in congenically-transferred untransduced (Ametrine neg.; red) Teff cells from
776 the same mouse. Background Rh123 efflux in untransduced Teff cells treated with the MDR1
777 inhibitor, elacridar, is shown in gray. Representative of 63 mice analyzed over 3-independent
778 experiments. **(d)** Mean normalized *ex vivo* Rh123 efflux ($\pm$ SEM) in FVB wild type spleen Teff cells
779 expressing control (*shCd8a*; *n* = 11) or CAR-targeting (shNr1i3) shRNAmirs; *shNr1i3.1* (*n* = 10),
780 *shNr1i3.2* (*n* = 10), *shNr1i3.3* (*n* = 12), *shNr1i3.4* (*n* = 10), *shNr1i3.5* (*n* = 10), determined by flow
781 cytometry as in (c). Rh123 efflux was normalized to control *shCd8a*-expressing Teff cells after
782 calculating the change (Δ) in Rh123 mean fluorescence intensity (MFI) between congenically-
783 transferred transduced (ametrine pos.) *vs*. untransduced (ametrine neg.) Teff cells. * $P < .05$, **** $P <$
784 $.0001$, One-way ANOVA with Dunnett's correction for multiple comparisons. **(e)** Mean relative
785 *Abcb1a*, *Nr1i3*, and *Cyp2b10* expression ($\pm$ SEM), determined by qPCR, in FVB spleen Teff cells
786 FACS-sorted from FVB.*Rag1*$^{-/-}$ recipient mice expressing either a negative control shRNAmir against
787 CD8 (*shCd8a*; *n* = 8), or the indicated shRNAmirs against CAR (*shNr1i3*s); *shNr1i3.1* (*n* = 8),
788 *shNr1i3.2* (*n* = 8), *shNr1i3.3* (*n* = 8), *shNr1i3.4* (*n* = 8), *shNr1i3.5* (*n* = 8).* $P < .05$, ** $P < .01$, *** P
789 $< .001$, **** $P < .0001$, One-way ANOVA with Tukey's correction for multiple comparisons. **(f)**

bioRxiv preprint doi: https://doi.org/10.1101/2020.07.30.229864; this version posted January 4, 2021. The copyright holder for this preprint (which was not certified by peer review) is the author/funder, who has granted bioRxiv a license to display the preprint in perpetuity. It is made available under aCC-BY-NC-ND 4.0 International license.

790 Median $\log_2$ fold change in shRNAmir abundance between FVB wild type *ex vivo*-isolated spleen *vs.*
791 *in vitro*-transduced (input) Teff cells. (a, d) shRNAmir abundance reflects the mean number of
792 normalized reads, by DNA-seq, in the indicated Teff subsets obtained in 2-independent screens, each
793 using cells transferred into 10 FVB.*Rag1*$^{-/-}$ mice. **(g)** *Ex vivo* Rh123 efflux, determined by flow
794 cytometry, in CD45.1 wild type (B6; red) or CD45.2 CAR-deficient (B6.*Nr1i3*$^{-/-}$), PXR-deficient
795 (B6.*Nr1i2*$^{-/-}$) or CAR/PXR double-deficient (B6.*Nr1i3*$^{-/-}$*Nr1i2*$^{-/-}$) effector/memory T cells (Teff; gated
796 as in Extended Data Fig. 6a; blue) isolated from spleens of B6.*Rag1*$^{-/-}$ mice 6-weeks post-naïve T cell
797 congenic co-transfer. Background Rh123 efflux in CD45.1 B6 Teff cells treated with the MDR1
798 inhibitor, elacridar, is shown in gray. Representative of a total of 22 mice analyzed over two-
799 independent T cell transfer experiments. **(h)** Mean normalized Rh123 efflux (+ SEM) in congenically-
800 transferred CD45.1 wild type (B6; n = 7) or CD45.2 CAR-deficient (B6.*Nr1i3*$^{-/-}$; n = 7), PXR-deficient
801 (B6.*Nr1i2*$^{-/-}$; n = 7) or CAR/PXR double-deficient (B6.*Nr1i3*$^{-/-}$*Nr1i2*$^{-/-}$; n = 7) spleen Teff cells,
802 determined by flow cytometry as in (g). * $P < .05$, One-way ANOVA with Tukey's correction for
803 multiple comparisons. **(i)** Mean relative *Abcb1a* expression (+ SEM), determined by *ex vivo* qPCR, in
804 CD45.1 wild type (B6; n = 5) or CD45.2 CAR-deficient (B6.*Nr1i3*$^{-/-}$; n = 5), PXR-deficient (B6.*Nr1i2*$^{-}$
805 $^{/-}$; n = 4) or CAR/PXR double-deficient (B6.*Nr1i3*$^{-/-}$*Nr1i2*$^{-/-}$; n = 5) spleen Teff cells (sorted as in
806 Extended Data Fig. 6a) from spleens of congenically-transferred B6.*Rag1*$^{-/-}$ as in (a). * $P < .05$, One-
807 way ANOVA with Tukey's correction for multiple comparisons.
808
809 **Extended Data Figure 2. Inhibition of bile acid reabsorption rescues ileitis induced by CAR-**
810 **deficient T cells in reconstituted *Rag*$^{-/-}$ mice.** **(a)** Mean weight loss (+SEM) of co-housed B6.*Rag2*$^{-/-}$
811 mice transplanted with wild type (B6; blue; n = 15) or CAR-deficient (B6.*Nr1i3*$^{-/-}$; red; n = 13) naïve
812 CD4^{+} T cells and treated with 2% (w:w) cholestyramine (CME) beginning at 3-weeks post-T cell
813 transfer. NS, not significant. **(b)** *Top*, H&E-stained sections of colons or terminal ilea from B6.*Rag2*$^{-/-}$
814 mice reconstituted with wild type or CAR-deficient T cells and treated +/- CME as in (a).
815 Representative of 12 mice/group. *Bottom*, mean histology scores (+ SEM; n = 12) for colons or
816 terminal ilea as in (a). NS, not significant. **(c)** Mean weight loss (+SEM) of co-housed B6.*Rag1*$^{-/-}$ mice
817 with or without the Apical sodium-dependent bile acid transporter (Asbt; gene symbol *Slc10a2*) after
818 transplantation with wild type (B6; blue) or CAR-deficient (B6.*Nr1i3*$^{-/-}$; red) naïve CD4^{+} T cells. **(d)**
819 *Top*, H&E-stained sections of terminal ilea or colons from control or Asbt-deficient B6.*Rag1*$^{-/-}$ mice
820 reconstituted with wild type or CAR-deficient T cells as in (c). Representative of 5 mice/group.
821 *Bottom*, mean histology scores (+ SEM; n = 5) for colons or terminal ilea as above. * $P < .05$, ** $P <$

bioRxiv preprint doi: https://doi.org/10.1101/2020.07.30.229864; this version posted January 4, 2021. The copyright holder for this preprint (which was not certified by peer review) is the author/funder, who has granted bioRxiv a license to display the preprint in perpetuity. It is made available under aCC-BY-NC-ND 4.0 International license.

822 .01, *** $P < .001$, One-way ANOVA with Tukey's correction for multiple comparisons. NS, not
823 significant.
824
825 **Extended Data Figure 3. Shared features of CAR-dependent gene expression in mucosal T cells**
826 **and hepatocytes.** **(a)** Overlap, presented as Venn diagrams, between genes induced in B6 wild type
827 mouse hepatocytes by *in vivo* treatment with either the mouse CAR agonist, TCPOBOP (TC) or the
828 mouse PXR agonist, PCN, relative to vehicle (CO, corn oil). **(b)** Enrichment of genes induced by TC,
829 but not PCN, treatment in mouse hepatocytes (as in [a]), within those reduced in CAR-deficient
830 (B6.*Nr1i3*$^{-/-}$) *vs*. wild type (B6) siLP Teff cells from week-3 congenically co-transferred *Rag1*$^{-/-}$ mice
831 (as in Fig. 2a-c). **(c)** Differential gene expression, determined by DEseq2 and shown as a volcano plot,
832 between CAR-deficient (B6.*Nr1i3*$^{-/-}$) and wild type (B6) siLP Teff cells re-isolated from transferred
833 B6.*Rag1*$^{-/-}$ mice, as in Fig. 2a. Genes induced by TC, but not PCN, treatment in mouse hepatocytes (as
834 in [a]; purple), bound by CAR in ChIP-seq analysis of hepatocytes from TC-treated mice (blue), or
835 both (red) are highlighted. Chi-square P values are indicated. **(d)** CAR-occupancy, determined by
836 ChIP-seq, at representative loci whose expression is regulated by CAR in both mucosal T cells and
837 hepatocytes within mouse hepatocytes ectopically expressing epitope-tagged mouse (m) or human (h)
838 CAR proteins and re-isolated from mice after treatment with the mCAR agonist, TCPOBOP (TC), or
839 the hCAR agonist, CITCO. * $P < 0.00001$; significant binding peaks were called in MACS using base
840 settings.
841
842 **Extended Data Figure 4. CAR promotes effector T cell persistence in the presence of small**
843 **intestinal bile acids**. **(a)** Percentages of live CD44^{hi} wild type (B6; CD45.1^{+}; blue) or CAR-deficient
844 (B6.*Nr1i3*$^{-/-}$; CD45.1^{-}; red) effector/memory (Teff) cells, determined by flow cytometry and gated as in
845 Extended Data Fig. 6a, in tissues of reconstituted B6.*Rag1*$^{-/-}$ mice over time. Numbers indicate
846 percentages; representative of 5 mice per tissue and timepoint. **(b)** Fitness, defined as mean $\log_2$ fold-
847 change (F.C.) of CAR-deficient (B6.*Nr1i3*$^{-/-}$) *vs*. wild type (B6) Teff cell percentages ($\pm$ SEM; $n = 5$)
848 in tissues of congenically co-transferred *Rag1*$^{-/-}$ mice over time, determined by flow cytometry as in
849 (a). **(c)** Percentage of wild type (B6, CD45.1^{+}; blue) and CAR-deficient (B6.*Nr1i3*$^{-/-}$, CD45.1^{-}; red)
850 naïve (CD62L^{hi}) CD4^{+} T cells after sorting and mixing, and prior to *in vivo* transfer into *Rag1*$^{-/-}$ mice
851 (input Tnaive); representative of 3 mixtures used for analyzing resulting Teff cells at 2- 4- or 6-weeks
852 post-transfer. **(d)** Equal numbers of CD45.1 wild type (B6; blue) and CD45.2 CAR-deficient
853 (B6.*Nr1i3*$^{-/-}$; red) naïve CD4^{+} T cells were transferred together into co-housed *Rag1*$^{-/-}$ mice with or
854 without the ileal bile acid reuptake transporter, Asbt (gene symbol *Slc10a2*). Resulting effector (Teff)

bioRxiv preprint doi: https://doi.org/10.1101/2020.07.30.229864; this version posted January 4, 2021. The copyright holder for this preprint (which was not certified by peer review) is the author/funder, who has granted bioRxiv a license to display the preprint in perpetuity. It is made available under aCC-BY-NC-ND 4.0 International license.

855 cells from small intestine lamina propria (siLP) were analyzed 2-weeks post- T cell transfer via flow
856 cytometry. **(e)** Percentages of live CD44^{hi} wild type (B6; CD45.1^{+}; blue) or CAR-deficient (B6.*Nr1i3*$^{-/-}$
857 ; CD45.1^{-}; red) effector/memory (Teff) cells, determined by flow cytometry and gated as in Extended
858 Data Fig. 6a, in siLP of week-2 reconstituted B6.*Rag1*$^{-/-}$ mice. Numbers indicate percentages;
859 representative of 8-10 mice analyzed over two-independent experiments. **(f)** Mean absolute numbers (±
860 SEM) of live CD45.1 wild type (B6; *left*) or CD45.2 CAR-deficient (B6.*Nr1i3*$^{-/-}$; *right*) Teff cells,
861 determined by *ex vivo* flow cytometry as in (e), from siLP 2-weeks after mixed T cell transfer into
862 control (Asbt$^{+/+}$; blue; n = 8) or Asbt-deficient (Asbt$^{-/-}$; red; n = 10) *Rag1*$^{-/-}$ recipients. Fold-changes in
863 cell numbers recovered from Asbt-deficient *vs*. control recipients, as well as P values (two-tailed
864 unpaired student's t test) are indicated.
865
866 **Extended Data Figure 5. Preferential CAR expression and function in human effector/memory T**
867 **cells expressing small bowel homing receptors. (a)** FACS-based identification of human CD4^{+} T cell
868 subsets in PBMC from healthy adult human donors. Expression of integrin α4 (α4 int.) in gated naïve
869 (gray), T regulatory (Treg; blue), or effector/memory (Teff; red) T cells is shown at right. **(b)**
870 Expression of integrin β7 (β7 int.) and CCR9 in total naïve CD4^{+} T cells, or in α4 int.+/- Treg or Teff
871 subsets (gated as in (a)). Representative of 13-independent experiments using PBMC from different
872 donors. **(c)** Percentages (%) of α4^{+}β7^{+}CCR9^{+} Tnaive, Treg, or Teff cells, determined by flow
873 cytometry as in (a-b). Individual data points for the 13 independent experiments are shown and
874 connected by grey lines. ** P < .01, One-way ANOVA with Holm-Sidak's correction for multiple
875 comparisons. **(d)** *Ex vivo* Rh123 efflux in CD4^{+} T cell subsets (gated as in a-b) in the presence (gray)
876 or absence (red) of the selective MDR1 inhibitor, elacridar. Representative of 8 experiments. **(e)** Mean
877 percentages (± SEM; n = 7) of Rh123^{lo} (MDR1^{+}) Teff subsets, determined by flow cytometry as in (d).
878 * P < .05, ** P < .01, *** P < .001, One-way ANOVA with Tukey's correction for multiple
879 comparisons. **(f)** Mean (± SEM) *ex vivo* expression, determined by qPCR, of CAR/*NR1I3* (n = 12),
880 MDR1/*ABCB1* (n = 12) or *CYP2B6* (n = 10) in α4^{-}β7^{-}CCR9^{-} or α4^{+}β7^{+}CCR9^{+} Tnaive, Treg or Teff
881 cells, FACS-sorted as in (a-b). (e-f) * P < .05, ** P < .01, One-way ANOVA with Tukey's correction
882 for multiple comparisons. **(g)** Mean relative *CYP2B6* expression (± SEM; n = 5), determined by qPCR,
883 in CD4^{+} T cell subsets (as in (f)) activated *ex vivo* with anti-CD3/anti-CD28 antibodies in the presence
884 or absence of titrating concentrations of the human CAR agonist, CITCO. Gene expression was
885 analyzed 24 hr post-activation. *** P < .001, Two-way ANOVA. **(h)** Mean normalized MDR1/*ABCB1*
886 or *CYP2B6* expression (± SEM), determined by RNA-seq and presented as transcripts per million

bioRxiv preprint doi: https://doi.org/10.1101/2020.07.30.229864; this version posted January 4, 2021. The copyright holder for this preprint (which was not certified by peer review) is the author/funder, who has granted bioRxiv a license to display the preprint in perpetuity. It is made available under aCC-BY-NC-ND 4.0 International license.

887 (TPM), in FACS-sorted $\alpha4^+\beta7^+$CCR9$^+$ Teff cells stimulated *in vitro* (anti-CD3/anti-CD28) for 24 hr in
888 the presence or absence of CITCO. Data from 4 replicate RNA-seq experiments are shown; ** $P <$
889 $.001$, paired two-tailed student's t test. **(i)** Identification of CD4$^+$ naive (Tnaive; CD25$^-$CD45RO$^-$; grey)
890 or effector/memory (Teff; CD25$^-$CD45RO$^+$; red) cells, by flow cytometry, from healthy adult human
891 PBMC. For improved purity of Th1, Th2, Th17 and Th17.1 cells, CCR10-expressing Th22 cells were
892 excluded. CCR6 expression in Tnaive (grey) or non-Th22 Teff cells (red) is shown at right; CCR6$^+$ or
893 CCR6$^-$ Teff cells were gated to enrich for Th17 or non-Th17 lineages, respectively. **(j)** Expression of
894 CCR4 and CXCR3 in CCR6$^-$ (non-Th17; *left*) or CCR6$^+$ (Th17; *right*) Teff cells identifies enriched
895 CCR6$^-$CCR4^{lo}CXCR3^{hi} (Th1; orange), CCR6$^-$CCR4^{hi}CXCR3^{lo} (Th2; blue), CCR6$^+$CCR4^{hi}CXCR3^{lo}
896 (Th17; green), and CCR6$^+$CCR4^{lo}CXCR3^{hi} (Th17.1; red) subsets. **(k)** Expression of integrin $\alpha4$ ($\alpha4$
897 int.; *top*) in Th2, Th1, Th17 and Th17.1 human Teff cells gated as in (a-b). Expression of integrin $\beta7$
898 ($\beta7$ int.) and CCR9 within $\alpha4$ int$^-$ (*middle*) or $\alpha4$ int$^+$ (*bottom*) Th2, Th1, Th17 or Th17.1 cells gated as
899 above. (a-c) Representative of 9-independent experiments using PBMC from different healthy adult
900 donors. **(l)** Percentages ($n = 9$) of $\alpha4^+\beta7^+$CCR9$^+$ cells within *ex vivo* Th1, Th2, Th17, or Th17.1 Teff
901 cells gated as in (a-c). Data from independent donors are connected by black lines. **(m)** MDR1-
902 dependent Rh123 efflux in the indicated Th1, Th2, Th17, or Th17.1 Teff subsets gated based on
903 expression of $\alpha4$ int., $\beta7$ int., and/or CCR9 in the presence (grey) or absence (red) of elacridar.
904 Representative of 8 independent experiments using PBMC from different donors. **(n)** Mean
905 percentages ($\pm$ SEM; $n = 8$) of Rh123^{lo} (MDR1$^+$) cells within Th1, Th2, Th17, or Th17.1 Teff subsets
906 gated based on expression of $\alpha4$ int., $\beta7$ int., and/or CCR9 as in (e). * $P < .05$, ** $P < .01$, *** $P <$
907 $.001$, One-way ANOVA with Tukey's correction for multiple comparisons. ND, not detectable; NS,
908 not significant.
909
910 **Extended Data Figure 6. TCPOBOP promotes CAR-dependent gene expression in *ex vivo*-**
911 **isolated effector T cells. (a)** *Top left,* equal numbers of CD45.1 wild type (B6; blue) and CD45.2
912 CAR-deficient (B6.*Nr1i3*$^{-/-}$; red) naïve CD4$^+$ T cells were transferred together into B6.*Rag1*$^{-/-}$ mice.
913 Resulting effector (Teff) cells were FACS-purified from spleen after 3 weeks. *Right*, sequential gating
914 strategy for re-isolating wild type and CD45.2 CAR-deficient spleen Teff cells is shown. *Bottom left*,
915 mean relative *Abcb1a*, *Cyp2b10*, or *Il10* expression ($\pm$ SEM; $n = 4$), determined by qPCR, in *ex vivo*-
916 isolated wild type (B6) or CAR-deficient (B6.*Nr1i3*$^{-/-}$) spleen Teff cells. These cells were used for *ex*
917 *vivo* cell culture experiments in the presence or absence of small molecule ligands ([b-c] below). * $P <$
918 $.05$, ** $P < .01$, paired two-tailed student's t test. **(b)** Mean relative expression ($\pm$ SEM) of *Abcb1a* ($n =$

bioRxiv preprint doi: https://doi.org/10.1101/2020.07.30.229864; this version posted January 4, 2021. The copyright holder for this preprint (which was not certified by peer review) is the author/funder, who has granted bioRxiv a license to display the preprint in perpetuity. It is made available under aCC-BY-NC-ND 4.0 International license.

919 4), *Cyp2b10* (n = 4), or *Il10* (n = 3), determined by qPCR, in wild type (B6) or CAR-deficient
920 (B6.*Nr1i3*$^{-/-}$) Teff cells isolated from transferred *Rag1*$^{-/-}$ mice (as in [a]), and stimulated *ex vivo* with
921 anti-CD3/anti-CD28 antibodies (for 24 hr) in the presence or absence of the mouse (m)CAR agonist,
922 TCPOBOP (TC; 10 μM), the mCAR inverse agonist, 5α-Androstan-3β-ol (And; 10 μM), or both. **
923 P < .01, *** P < .001, **** P < .0001, one-way ANOVA with Tukey's correction for multiple
924 comparisons. **(c)** Mean relative *Abcb1a*, *Cyp2b10*, or *Il10* expression (+ SEM; n = 5), determined by
925 qPCR, in wild type (B6) or CAR-deficient (B6.*Nr1i3*$^{-/-}$) Teff cells isolated and stimulated as in (a-b) in
926 the presence or absence of TC (10 μM) or the mouse PXR agonist, PCN (10 μM). Data are presented
927 as fold-change in mRNA abundance relative to vehicle-treated cells (DMSO for TC; ethanol for PCN).
928 **** P < .0001, one-way ANOVA with Dunnett's correction for multiple comparisons. NS, not
929 significant.
930

931 **Extended Data Figure 7. Characteristics of endogenous intestinal metabolites that activate the**
932 **CAR ligand-binding domain. (a)** Mean activation (+ SEM; triplicate samples) of recombinant human
933 (h)RXRα ligand-binding domain (LBD) homodimers, determined by time-resolved fluorescence
934 resonance energy transfer (TR-FRET), in the presence of the mCAR agonist, TCPOBOP (TC; blue) or
935 the hRXRα agonist, 9-*cis* retinoic acid (RA; red). Median effective concentration (EC_{50}) of 9-*cis* RA-
936 dependent hRXRα LBD homodimer activation is indicated. Representative of more than 5-
937 independent experiments. **(b)** Mean activation (+ SEM; n = 3) of hRXRα LBD homodimers,
938 determined by TR-FRET as in (a), in the presence of titrating concentrations of siLC, bile, cLC or
939 serum from wild type B6 mice. * P < .05, **** P < .0001, one-way ANOVA with Tukey's correction
940 for multiple comparisons. NS, not significant. **(c)** Mean activation (+ SEM; n = 3) of CAR:RXR LBD
941 heterodimers, determined by TR-FRET, in the presence of titrating concentrations of siLC isolated
942 from conventionally-housed (Conv) or germ-free (GF) wild type B6 mice pre-treated with or without
943 cholestyramine (CME) to deplete free bile acids. *** P < .001, **** P < .0001, One-way ANOVA
944 with Dunnett's correction for multiple comparisons. (a-c) The bars for each tissue extract indicate
945 dilution series *(left to right)*: (1) diluent (PBS) alone; (2) 0.01%, (3) 0.1%, and (4) 1%. Data are shown
946 from 3-independent experiments using extracts from different wild type mice, with each concentration
947 from each individual mouse run in triplicate. **(d)** Mean TR-FRET signals (+ SEM; n = 3) of CAR:RXR
948 LBD heterodimers in the presence of titrating concentrations of individual bile acid (BA) species. NS,
949 not significant, one-way ANOVA with Dunnett's correction for multiple comparisons. The bars for
950 BAs indicate concentrations *(left to right)*: (1) vehicle (DMSO); (2) 10 μM; (3) 100 μM; and (4) 1000

bioRxiv preprint doi: https://doi.org/10.1101/2020.07.30.229864; this version posted January 4, 2021. The copyright holder for this preprint (which was not certified by peer review) is the author/funder, who has granted bioRxiv a license to display the preprint in perpetuity. It is made available under aCC-BY-NC-ND 4.0 International license.

951 μM. Data are shown from 3-independent experiments, where each BA concentration was run in
952 triplicate.
953
954 **Extended Data Figure 8. CAR promotes IL-10 expression in mucosal Teff cells and regulates Tr1**
955 **and Th17 cell development in the small intestine.** **(a)** Equal numbers of CD45.1 wild type (B6;
956 blue) and CD45.2 CAR-deficient (B6.*Nr1i3*$^{-/-}$; red) naïve CD4^{+} T cells were transferred together into
957 *Rag1*$^{-/-}$ mice. Resulting effector (Teff) cells were analyzed—using surface and intracellular flow
958 cytometry after *ex vivo*-stimulation with phorbol myristate acetate (PMA) and ionomycin—at 2- 4- and
959 6-weeks from spleen, mesenteric lymph node (MLN), small intestine lamina propria (siLP), or colon
960 lamina propria (cLP). Gating hierarchy is shown from a representative sample of MLN mononuclear
961 cells at 2-weeks post-T cell transfer. **(b)** Intracellular IL-10 and IFNγ expression, determined by flow
962 cytometry, in wild type (B6, blue; *left*) or CAR-deficient (B6.*Nr1i3*$^{-/-}$, red; *right*) non-Th17 Teff cells,
963 gated as in (a), from tissues of T cell-reconstituted B6.*Rag1*$^{-/-}$ mice over time. Numbers indicate
964 percentages; representative of 5 mice per tissue and time point. Mean percentages **(c)** or numbers **(d)**
965 ($\pm$ SEM; n = 5) of IL-10-expressing wild type (B6, *left*) or CAR-deficient (B6.*Nr1i3*$^{-/-}$, *right*) Teff
966 cells, determined by *ex vivo* flow cytometry as in (a-b), from tissues of transferred B6.*Rag1*$^{-/-}$ mice
967 over time. **(e)** Specificity of IL-10 intracellular staining, as validated by analysis of IL-10 production
968 by CD45.1 wild type (B6; blue) or CD45.2 *Il10*$^{-/-}$ (red) Teff cells isolated from spleen or siLP of
969 congenically co-transferred *Rag1*$^{-/-}$ mice. Representative of 6 mice analyzed over 2-independent
970 experiments. **(f)** Expression of RORγt and IL-17A, determined by intracellular FACS analysis as in
971 Extended Data Figure 8a, in wild type (B6) or CAR-deficient (B6.*Nr1i3*$^{-/-}$) CD4^{+} effector/memory
972 (Teff) cells from tissues of reconstituted *Rag1*$^{-/-}$ mice 2-weeks post-mixed T cell transfer. Numbers
973 indicate percentages; representative of 5 mice per tissue and time point. **(g)** Mean percentages of ($\pm$
974 SEM; n = 5) wild type (B6; blue) or CAR-deficient (B6.*Nr1i3*$^{-/-}$; red) RORγt^{+}IL-17A^{-} Teff cells,
975 determined by intracellular flow cytometry as in (a). * $P < .05$, paired two-tailed student's t test. **(h)**
976 Expression of RORγt and IL-17A, determined by intracellular FACS analysis, in wild type (B6) or *Il10*
977 $^{-/-}$ Teff cells from tissues of reconstituted *Rag1*$^{-/-}$ mice 2-weeks post-mixed T cell transfer. Numbers
978 indicate percentages; representative of 5 mice per tissue and time point. **(i)** Mean percentages of ($\pm$
979 SEM; n = 7) wild type (B6; blue) or *Il10* $^{-/-}$ (red) RORγt^{+}IL-17A^{-} Teff cells, determined by intracellular
980 flow cytometry as in (c). * $P < .05$, ** $P < .01$, paired two-tailed student's t test. MLN, mesenteric
981 lymph nodes; siLP, small intestine lamina propria; cLP, colon lamina propria.
982

bioRxiv preprint doi: https://doi.org/10.1101/2020.07.30.229864; this version posted January 4, 2021. The copyright holder for this preprint (which was not certified by peer review) is the author/funder, who has granted bioRxiv a license to display the preprint in perpetuity. It is made available under aCC-BY-NC-ND 4.0 International license.

983 **Extended Data Figure 9. CAR expression and function in mucosal Teff cells is increased in**
984 **response to intestinal inflammation. (a)** Percentages of $CD3^+CD4^+$ T cells in tissues of *Rag1*$^{-/-}$ mice
985 transplanted with congenic mixtures of wild type and CAR-deficient naïve $CD4^+$ T cells over time,
986 determined by flow cytometry. Representative of 5 mice per tissue and time point. **(b)** Mean absolute
987 numbers of $CD3^+CD4^+$ T helper (T_H) cells ($\pm$ SEM; n = 5) in tissues of transferred B6.*Rag1*$^{-/-}$ mice
988 over time, determined by flow cytometry as in (a). **(c)** Mean relative *ex vivo* CAR (*Nr1i3*), MDR1
989 (*Abcb1a*), *Cyp2b10*, or *Il10* gene expression ($\pm$ SEM; n = 3), determined by qPCR, in wild type (B6)
990 $CD4^+$ effector/memory (Teff) cells (sorted as in Extended Data Fig. 8a) from spleens of transferred
991 B6.*Rag1*$^{-/-}$ mice over time. **(d)** *Top row*, expression of Foxp3 and RORγt, determined by intracellular
992 staining after *ex vivo* (PMA+ionomycin) stimulation, in $CD4^+CD44^{hi}$ cells from spleen (*left*) or small
993 intestine lamina propria (siLP, *right*) of wild type (B6, blue) or CAR-deficient (B6.*Nr1i3*$^{-/-}$, red) mice
994 injected with isotype control (IgG) or soluble anti-CD3. *Bottom 4 rows*, expression of IL-10 and IL-
995 17A in wild type or CAR-deficient spleen or siLP T cell subsets from mice treated +/- isotype control
996 (IgG) or anti-CD3 antibodies. Cells were gated and analyzed by flow cytometry as above. Numbers
997 indicate percentages; representative of 3 mice per group and genotype analyzed over 2-independent
998 experiments. **(e-f)** Mean percentages of IL-10-expressing T cell subsets ($\pm$ SEM; n = 3), gated and
999 analyzed by *ex vivo* flow cytometry as in (a), in spleen **(f)** or siLP **(e)** T_H cell subsets from wild type
1000 (B6, blue) or CAR-deficient (B6.*Nr1i3*$^{-/-}$, red) mice injected with or without isotype control (IgG) or
1001 anti-CD3 antibody. * $P < .05$, one-unpaired student's t test; some P values are listed directly.
1002
1003 **Extended Data Figure 10. TCPOBOP protection against bile acid-induced ileitis requires CAR**
1004 **expression in T cells. (a)** Mean weight loss ($\pm$ SEM; n = 5/group) of co-housed B6.*Rag2*$^{-/-}$ mice
1005 transplanted with CAR-deficient (B6.*Nr1i3*$^{-/-}$) $CD4^+$ naïve T cells and maintained on a CA-
1006 supplemented diet with (CA/TC) or without (CA/Veh) TC treatment. Weights are shown relative to 3-
1007 weeks post-transfer when TC treatments were initiated. NS, not significant; two-way ANOVA. **(b)**
1008 H&E-stained sections of terminal ilea or colons from B6.*Rag2*$^{-/-}$ mice reconstituted with CAR-
1009 deficient T cells and treated as above and as indicated. Representative of 5 mice/group. **(c)** Mean
1010 histology scores ($\pm$ SEM) for colons or terminal ilea as in (b). NS, not significant; paired student's t
1011 test.

Figure 1

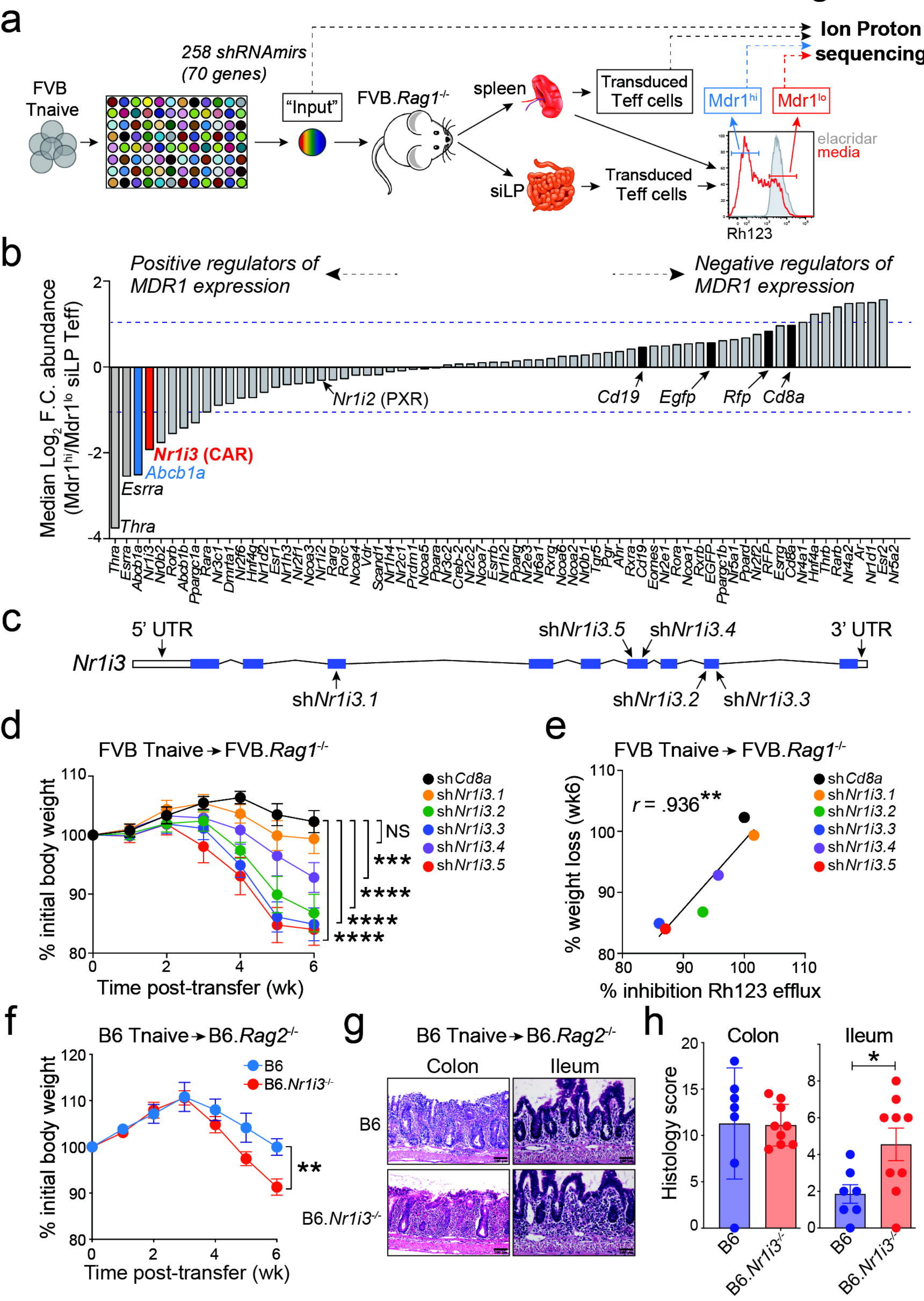

Figure 2

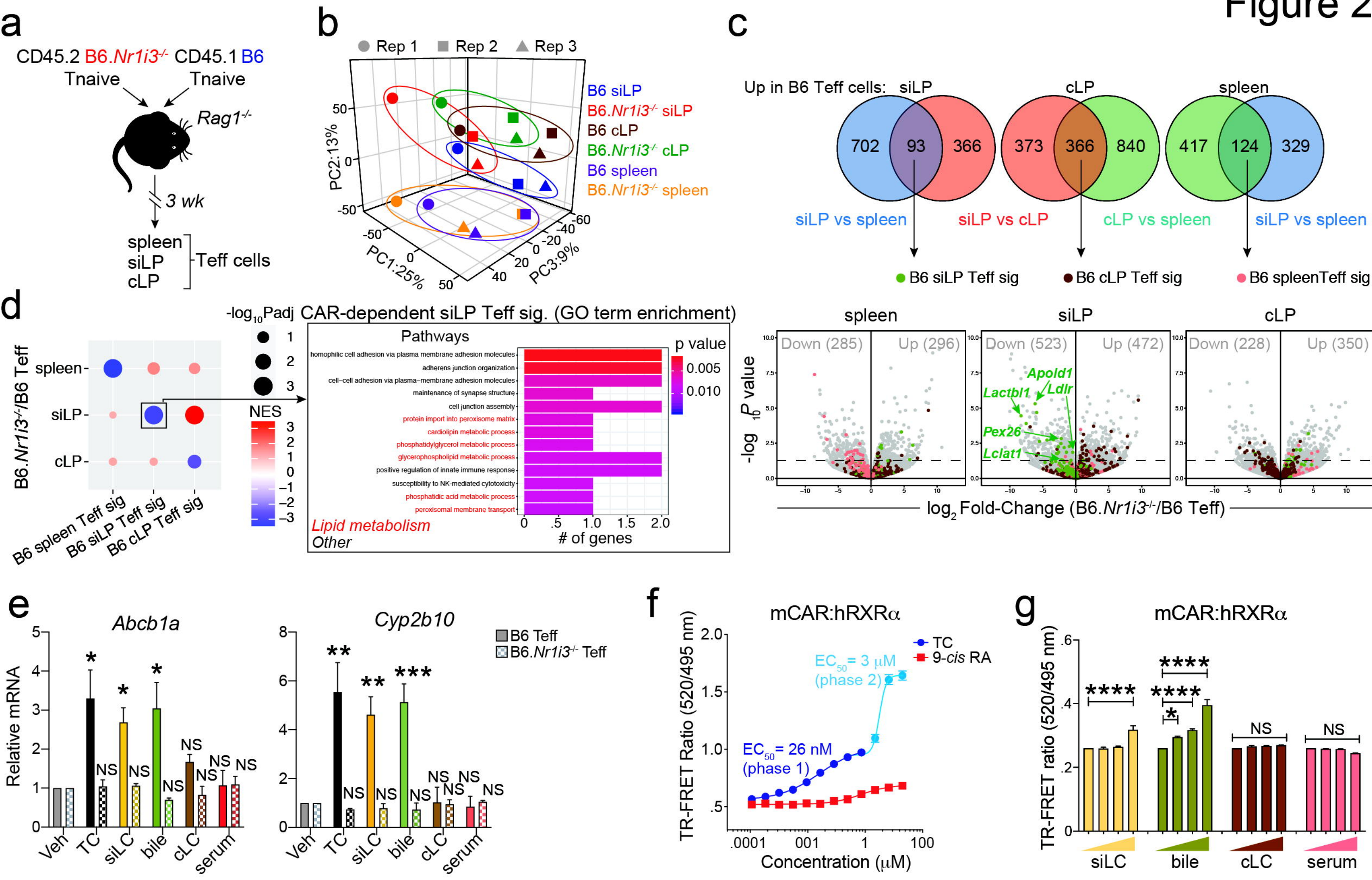

Figure 3

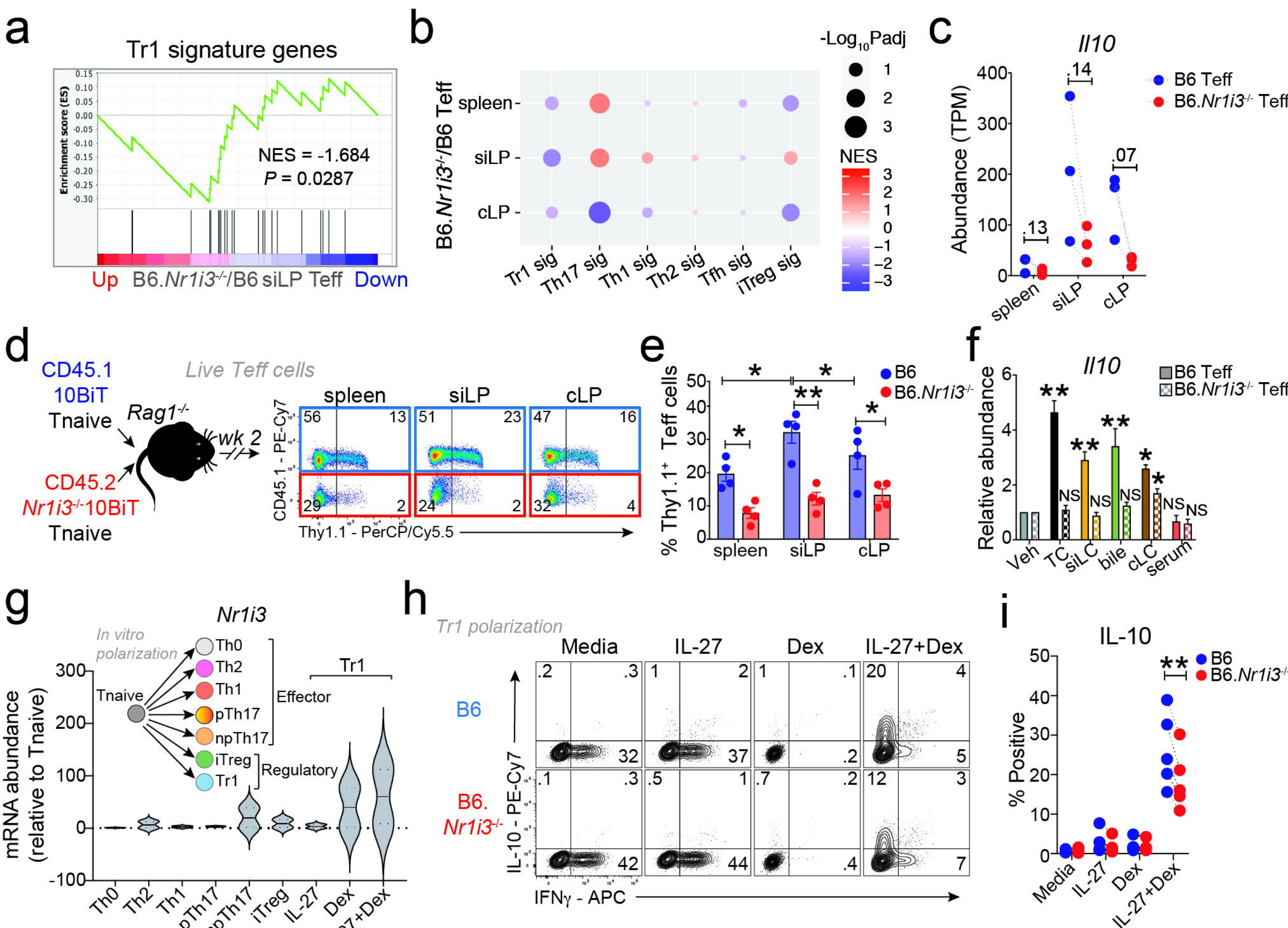

Figure 4